Drainage evolution in arid extensional settings and its controls on coral reef development: Sinai, Egypt

Hakan Heggernes

Master of Science thesis

Basin and Reservoir studies

Department of Earth Science

University of Bergen

June 2019

Abstract

The Sinai Peninsula is located in a hyper-arid climate environment, which affects drainage, development of coastal fan deltas and the growth of coral reef along the Gulf of Suez and Gulf of Aqaba. The recent extension of Gulf of Suez and the strike-slip tectonics of the Gulf of Aqaba give the possibility to contrast two different tectonic settings under the same arid conditions. The purpose of this study is to identify relationships and trends between catchment areas, fan deltas and coral reefs in the shallow-water area. Additionally two flash flood events, from 2002 and 2016, and the delivery of sediments to the coastal area have been studied.

This thesis is based on mapped catchments, fan deltas, coral reefs and shallow-water (to 5 m depth) areas. Mapping of the geomorphological features was done using ArcGIS, where catchments were extracted from a DEM, the fan deltas mapped and shallow-water bathymetry and coral reef area are derived from Landsat satellite images.

The drainage systems on the southern Sinai Peninsula are dominated by steep gradients, draining the high mountains of central Sinai. The catchments feed the coastal fan deltas with coarse-grained sediments, which build into the shallow-water areas around the fans, on top of which coral reefs, mostly fringing reefs, colonise. Coastal fans, coral reef and shallow-water areas are larger in the Gulf of Suez due to rotated normal-fault blocks, which are absent in the Gulf of Aqaba. In the study area larger fan deltas have larger areas occupied by coral reefs.

The sediments delivered to the coastal areas are delivered by infrequent, aperiodic flash flood events. Such events can be destructive for coral reefs. The fan deltas usually have well-defined distributary channels transporting most of the sediments past the coral reefs and depositing most of it in the area corresponding to 4-5 m water depth. In addition, marine currents quickly remove the sediments deposited by after the flash floods, minimising damage to coral reefs.

Acknowledgements

This study was conducted at the Department of Earth Science, University of Bergen, during the period 2017-2019, as part of a master degree in Basin and Reservoir studies.

I would like to thank my supervisor, Martin Muravchik, for all the helpful guidance, comments and feedback during this master project. I would also like to thank Martin for all the help regarding ArcGIS. I would also like to thank my co-supervisor, Bjørn Nyberg, for additional help with ArcGIS and for comments and feedback on my thesis.

I would like to thank friends and family who took the time to read through parts or my entire thesis. Comments on grammar have been much needed and very helpful.

Last but not least I would like to thank my fellow students at the University of Bergen for five amazing years. A special thanks to the students who I shared Grotten and Gneis with, for all the good times.

Bergen 2. June 2019
Hakan Heggernes

Contents

1 INTRODUCTION

1.1 Rationale

In order to better understand the development of sedimentary systems and depositional environments in extensional basins, it is crucial to understand the tectonic controls on both the sediment source area and the depositional area. Existing geological models of such basins are highly biased towards relatively wet climate regimes. The climate controls temperature and precipitation within drainage systems, which again control elements like erosion rates and water and sediment discharge. The Sinai Peninsula in Egypt makes it possible to analyse how sedimentary systems, drainage pattern and depositional environments are controlled by a hyper-arid climate. Additionally, in this it is possible to compare and contrast the effects on two different tectonic settings under the same climate conditions: the recent extensional setting of the Gulf of Suez and the active strike-slip tectonics of the Gulf of Aqaba.

The Red Sea, Gulf of Suez and Gulf of Aqaba have been the focus of several studies investigating rift evolution of early rift basins and tectonic controls on sedimentary deposition and distribution. However, little attention has focused on development of coral reef systems in arid extensional and strike-slip settings. The study by Rowlands et al. (2014) looked at carbonate systems along the Saudi Arabian Red Sea coast, relating tectonic and sedimentary controls to coral reef distribution. This study will take a similar approach on the southern coasts of the Sinai Peninsula and investigate controls on coastal fan delta development and coral growth.

1.2 Project aims

The main purpose of this study is to analyse the drainage pattern of the Sinai Peninsula and the coastal environment to identify controls on drainage, deposition and coral reef growth. The particular aims are as follows

- Analyse the geomorphology of the catchments draining the Sinai Peninsula.
- Map and analyse coastal fan deltas along the Sinai Gulf of Suez and Gulf of Aqaba coasts.

- Use satellite derived bathymetry to analyse the shallow-water areas and coral reef distribution on the coastal fan deltas.
- Identify tectonic, sedimentological and environmental controls on drainage systems, fan delta development and coral reef growth.
- Analyse and identify relationships between geomorphological features and depositional systems.
- Compare results between the Gulf of Suez and the Gulf of Aqaba.

1.3 Study area

The Sinai Peninsula is located in the North-eastern parts of Egypt, on the border to Israel and Saudi-Arabia. The Sinai Peninsula consists of high ranging mountains (>2500 m), which quite steeply plunge into the Gulf of Suez and the Gulf of Aqaba. The Gulf of Suez is an abandoned rift arm extending northwest from the Red Sea, whereas Gulf of Aqaba extends north from the Red Sea, with the Sinai Peninsula placed in between, as shown on Figure 1.1.

1.4 Methods

This study uses remote sensing techniques to extracts geomorphological features from the Sinai Peninsula. The study combines a digital elevation model of the Sinai Peninsula with Landsat satellite images to describe and analyse the geomorphology of the Sinai Peninsula.

1.5 Thesis layout

This thesis is divided into seven chapters; **Chapter 2** contains the background, which introduces the topics and concepts that are central in this study; **Chapter 3** presents the geological setting; **Chapter 4** describes the methods and data used to do geomorphological analysis and Satellite derived bathymetry of the shallow-water areas; **Chapter 5** presents the results and finding of the study and examines relationships between studied features; **Chapter 6** discusses the results from chapter 5 and tries to explain identified relationships on distribution of costal fan deltas and coral reefs within the two basins; **Chapter 7** summarises the main findings from this study.

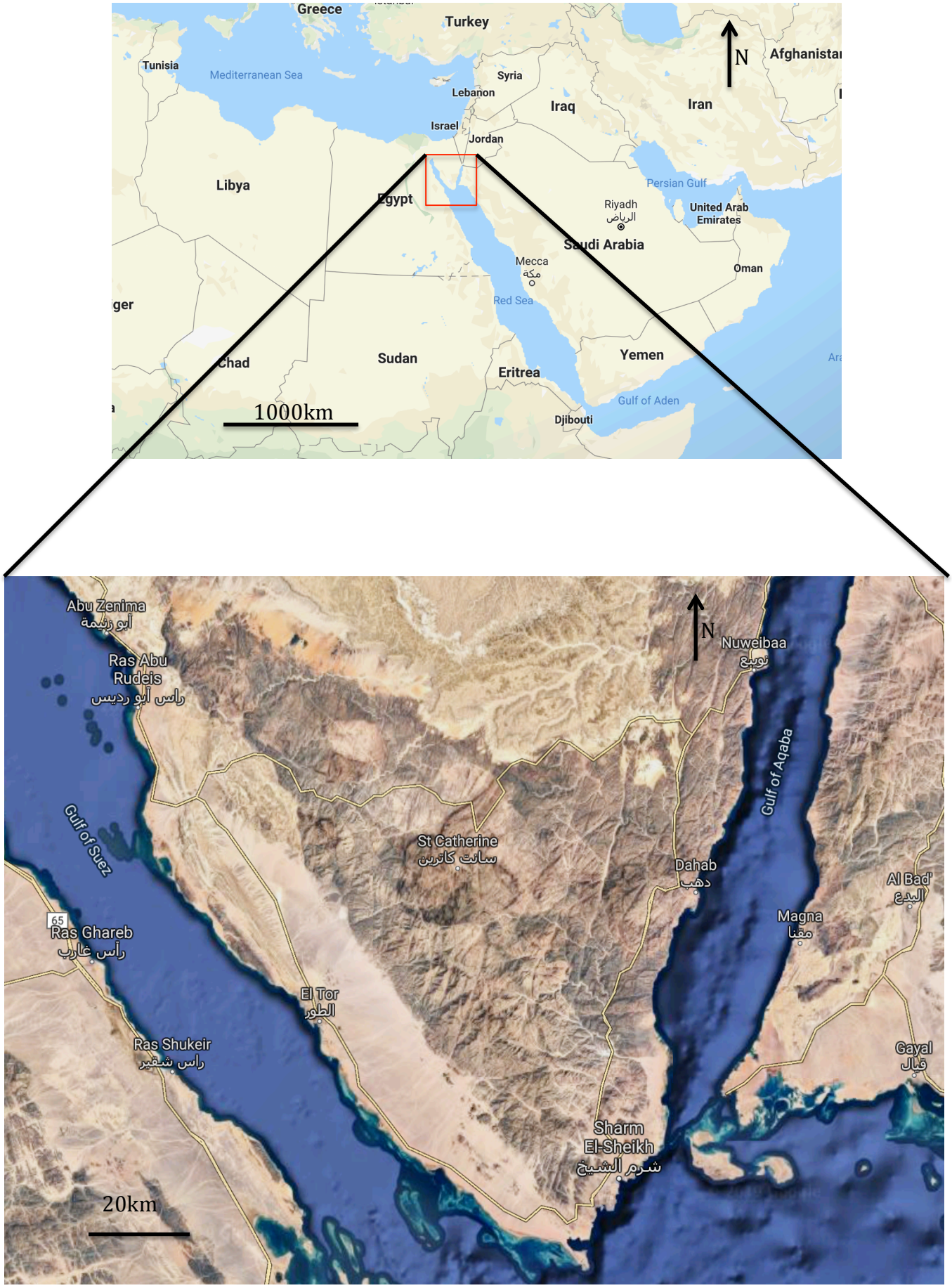

Figure 1.1 The study area is located on the southern part of the Sinai Peninsula in Egypt. The shallow-waters of the Sinai Gulf of Suez and Gulf of Aqaba coasts are also part of this study. From Google Maps.

2 BACKGROUND

The purpose of this chapter is to give short introductions to the topics that are central to this study. In order to understand how drainage networks and depositional environments evolve and behave in a rift setting, it is important to have an understanding of how rift basins evolve. Rift evolution is controlled by fault growth and fault linkage, which are the primary controls on drainage and depositional systems.

2.1 Evolution of Rift Basins

Rift basins are elongated geological features caused by the breaking up of the continental crust, bounded by normal faults (Nelson et al., 1992). These basins develop as a response to thinning and stretching of the lithosphere, causing depressions in the crust in form of graben structures (Dewey and Bird, 1970). Two end members have been identified as to how rift basins develop: active and passive rifting. Active rifting occurs when heat and magma from the mantle transfers to the crust, causing uplifting, thinning and break-up of the crust. Passive rifting, however, is related to tensional stresses within the lithosphere (crust and upper mantle) itself, causing the crust to thin and break up, leading to intrusion of magma into the crust as a response to the rifting (Allen and Allen, 2013). The tectonic plate will rupture along the central parts of the rift basin, as these areas of the crust have been subjected to the largest amounts of thinning and faulting. In addition, high volcanic activity is common in rift areas, with sills and dikes intruding bedrock and sediments (Dewey and Bird, 1970). Grabens within a rifting event tend to be asymmetrical, due to flanking fault blocks being rotated as the crust is stretched and broken up. Eventually, if this process of thinning and stretching of the tectonic plate continues undisturbed, the rift basin will be torn apart along its main fault, resulting in two continental plates, and new oceanic crust will be produced between them (Dewey and Bird, 1970). If, for some reason, the rifting stops along the process described, it is called a failed rift (Allen and Allen, 2013).

Rift systems typically develop in one of two ways: the rifting starts off in one area and propagates in one or more directions until it reaches its final size, or the whole length of the rift system is activated more or less simultaneously (Nelson et al., 1992). Either way, the rift basin does not consist of one large continuous fault, but rather several smaller fault segments that grow and interact with each other by linking and overlapping, with a single fault segment being in the range of 10s-100s km (Nelson et al., 1992; Gawthorpe and Leeder, 2000). It is the behaviour of normal faults that is the most important control on the spatial evolution and geometry of rift basins. Studies have shown that there is a relationship between the length and displacement on faults expressed in a growth law:

$$D = cL^n$$

Where D is displacement, L is length, c is a constant related to rock properties and n is a scaling exponent (Dawers and Anders, 1995; Gawthorpe and Leeder, 2000). This relationship suggests that normal fault and rift zones predominantly grow by smaller faults linking to become larger faults. It is also recognised that a few, major, through-going faults are responsible for most of the displacement within a rift zone (Dawers and Anders, 1995; Cowie et al., 2000; Gawthorpe and Leeder, 2000).

The development of a normal fault array can be divided into three stages: the initiation stage, the linkage and interaction stage and the through-going faults stage (Figure 2.1; Cowie et al., 2000; Gawthorpe and Leeder, 2000). The initiation stage involves a large number of small, individual fault segments with little displacement and little to no interaction between the faults. In the second stage, faults interact with each other and start linking together, with some faults growing larger and accumulating more displacement then other faults. The final stage is described as a few faults growing until they cut through the full length of the rift zone, whereas small faults become inactive (Figure 2.1; Cowie et al., 2000; Gawthorpe and Leeder, 2000).

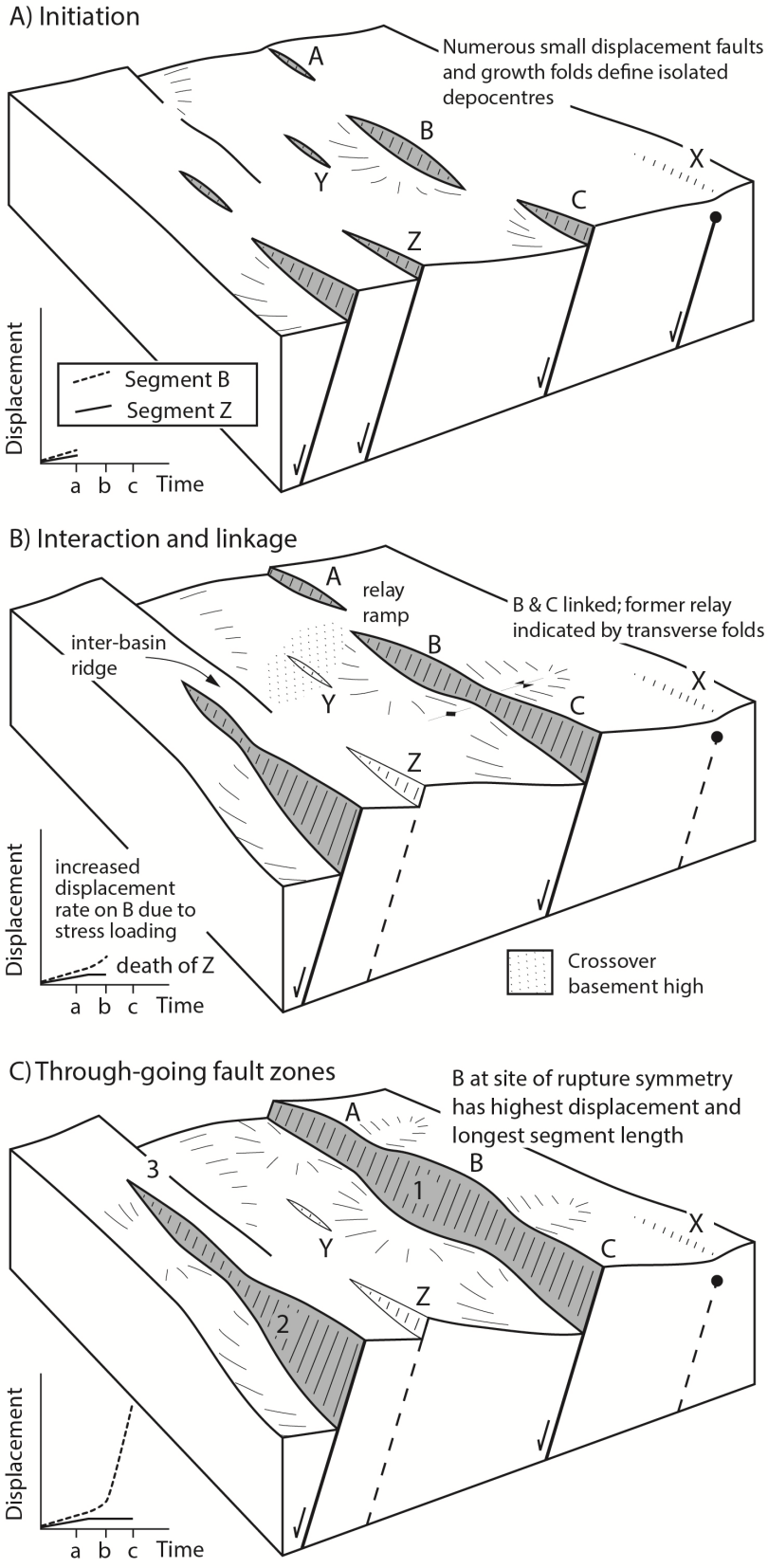

Figure 2.1 The evolution of rift basins can be devided in three stages: a) initiation stage, b) interaction and linking stage and c) through-going faults stage. From Gawthorpe and Leeder (2000).

2.2 Drainage Development and Characteristics in Rift Basins

The spatial arrangement of the fault network in a rift zone is the main control on the geometrical, topographical and morphological evolution of a rift basin, which are important controls on drainage development in active rift basins (Leeder and Jackson, 1993; Gawthorpe and Leeder, 2000; Cowie et al., 2006). Fault segments differ in size, displacement and slip rate (Cowie et al., 2006). Areas where faults do not link but rather overlap is called a relay ramp or a transfer zone and are areas of less displacement along the length of a fault, forming topographic lows along the fault (Gawthorpe and Hurst, 1993; Jackson and Leeder, 1994). This complexity of fault evolution is what controls the drainage network within a rift basin. Fault development controls the size of catchment areas and accommodation space, and thus controlling sediment deposition and distribution of alluvial fan and fan deltas (Gawthorpe and Hurst, 1993; Eliet and Gawthorpe, 1995; Gawthorpe and Leeder, 2000).

It can be distinguish between two types of drainage patterns within a rift basin: axial drainage and transverse drainage (Ravnås and Steel, 1998; Gawthorpe and Leeder, 2000). Axial drainage systems are oriented parallel to the strike of the rift axis, and are located in the topographic lows between two bounding faults. Transverse drainage, however, are oriented perpendicular to the strike of the rift axis and can cut thorough the fault scarp (Gawthorpe and Leeder, 2000). Transverse drainage can be further divided into two types: large hinterland catchments and small footwall catchments (Cowie et al., 2006). Within a rift basin there are usually a few hinterland catchments that drain large areas (>100 km^2) behind the basin bounding faults. In comparison, the footwall catchments are small in size, quite steep and are located on the footwall scarp (Eliet and Gawthorpe, 1995; Cowie et al., 2006).

Usually fault growth dictates the drainage pattern, where streams seek low-points in the topography such as areas between fault tips, transfer zones and relay ramps (Figure 2.2; Gawthorpe and Leeder, 2000; Cowie et al., 2006). In some cases antecedent drainage occurs, which is drainage pattern that existed prior to faulting and rifting and is inherited through the evolution of the rift

basin (Eliet and Gawthorpe, 1995). Such drainage systems have enough erosive power to incise into uplifting footwalls, maintaining their pre-rift course. If the drainage system does not have the erosive power to keep up with the uplifting fault blocks and the generation of new slopes, streams will be redirected to a new path or completely reversed (Eliet and Gawthorpe, 1995). Figure 2.2 is an example of how drainage might respond to fault growth and illustrates how the surface response can creates one large catchment area, and several smaller catchments on the footwall scarp.

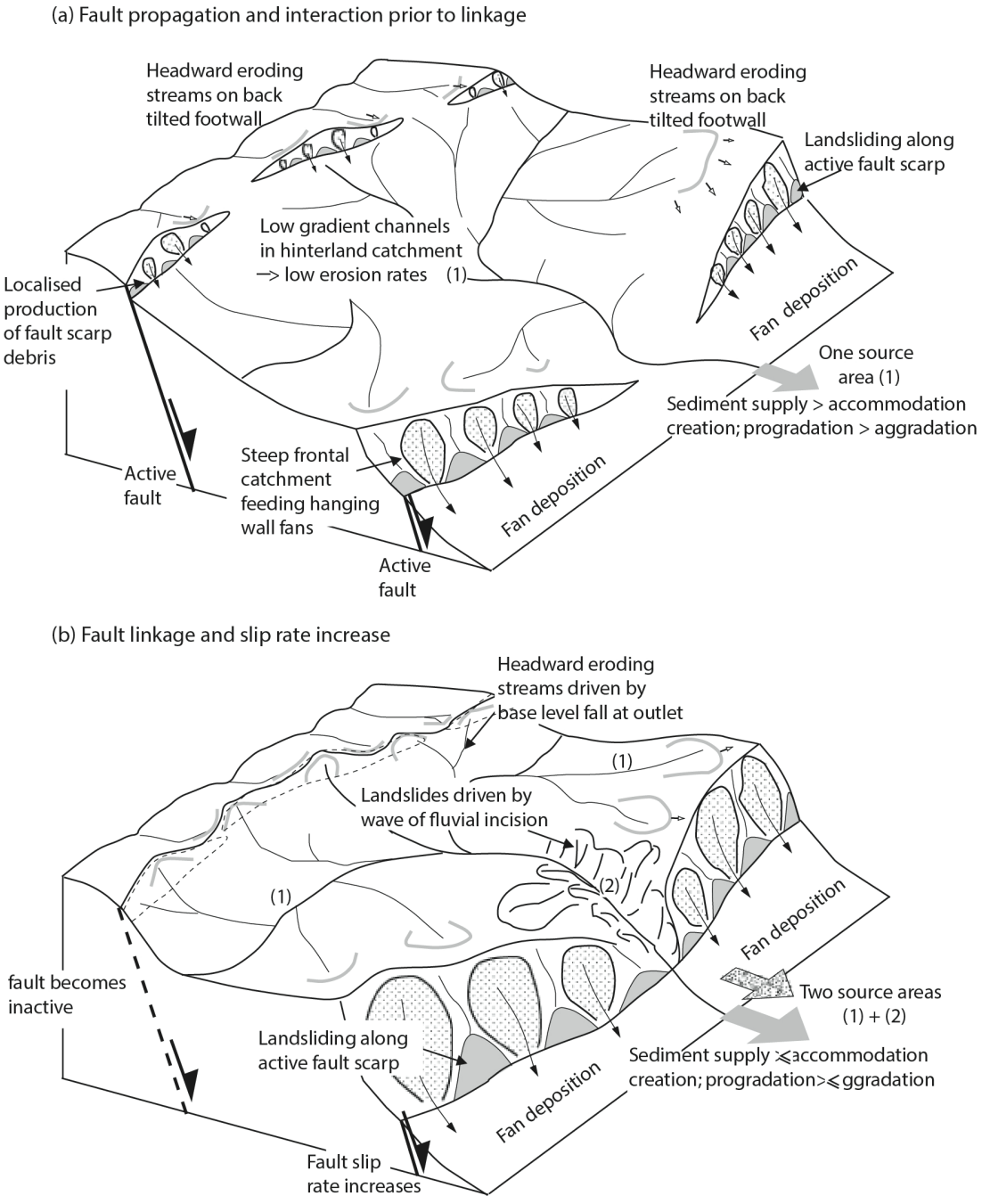

Figure 2.2 Illustration of surface response as faults link and grow. a) Showing how the drainage takes advantage of the topographic low created between two growing fault segments in the initiation stage. B) Shows the drainage response as the faults link and create though-going faults, maintaining its path from the initiation stage and creating an incision into the footwall. From Cowie et al. (2006).

2.3 Climate Controls

While the fault arrangement is the primary control on the morphology and geometry of rift basins, drainage area and drainage pattern, climate is one of the major controls on the sedimentary systems and depositional environments (Ravnås and Steel, 1998; Gawthorpe and Leeder, 2000). The climate controls the seasonal variations on precipitation, temperature variations and wind levels. These factors affect erosion rates, weathering rates, vegetation and biomass development, thus controlling the depositional environments (Ravnås and Steel, 1998; Gawthorpe and Leeder, 2000). In addition, the erodability of the lithology within the drainage systems will affect the sediment supply, as harder rock types, like metamorphic bedrock, are more difficult to erode and sedimentary rock, like sandstone, erode more easily (Ravnås and Steel, 1998). Temperature and precipitation are also important for erosion and sediment transportation (Syvitski and Milliman, 2007). Higher temperatures and precipitation within a drainage basin are usually linked with an increase in weathering, dissolving and erosion rates (Dupré et al., 2003).

2.4 Coarse-grained fan deltas

Coarse-grained deltas are common depositional systems in rift basins (Gawthorpe and Colella, 1990; Young et al., 2000). Rift basins tend to have steep slopes generated by the steep footwall scarps of normal faults, with accommodation space being created by the uplifting footwall and the subsiding hanging-wall (Gawthorpe and Colella, 1990; Eliet and Gawthorpe, 1995). Steep mountainsides generate high erosive power to water flow, which will carry coarser grain sizes (medium to coarse sand and conglomerate). In marine basins the sediments are deposited in coarse-grained fan deltas in the coastal zone where the steep drainage systems meet the marine environment, i.e. deltas develop in close proximity to its source, depositing coarse-grained, unsorted fan deltas (Gawthorpe and Colella, 1990; Nir, 1996). The slope of the footwall scarp tend to dip steeply, whereas hanging-wall slopes have gentler dip (Gawthorpe and Colella, 1990). This result in coarse-grained fan deltas deposited on the hanging-wall that tend to be laterally more extensive than fan deltas derived from the footwall scarp (Gawthorpe and Colella, 1990).

2.5 Coral development

Coral growth and carbonate production in arid extensional settings like the Red Sea tend to develop in warm, clear, shallow (< 30 m) waters, where there is little to no siliciclastic input (e.g. Purser et al., 1987; Hay et al., 1988; Fabricius, 2005; Rowlands et al., 2014). Location and distribution of coral reefs is highly dependent on basin topography, where corals can develop attached to the coastal zone or detached as offshore platforms (e.g. Bosence, 2005). In marine rift basins, where steep drainage systems typically flank the basin, coral formation is dependent on an arid climate to minimise siliciclastic stress on the corals and keeping clear water (Gawthorpe and Colella, 1990; Dullo and Montaggioni, 1998). Coral development in rift settings is highly dependent on tectonics to create environments for corals to grow (Dullo and Montaggioni, 1998; Bosence, 2005). Corals can develop along the basin margins, atop rotating fault blocks or salt diapirs, where the last two can create topographic highs in central parts of a rift basin for coral reefs to form detached platforms (Roberts, 1987; Bosence, 2005). Further explanation of coral reefs in the Red Sea, Gulf of Suez and Gulf of Aqaba in section 3.5.

2.6 Landsat 8 satellite imagery

Satellite derived bathymetry is a method that uses multispectral satellite imagery to estimate shallow-water bathymetry. The Landsat missions are one of the most frequently used sources of data for this kind of analysis as the imagery is free and publicly available via the U.S. Geological Survey. In this study the satellite imagery of the Landsat 8 mission were used, which provides images with 30 m spatial resolution. The Landsat 8 dataset consists of 11 bands corresponding to different intervals of the electromagnetic spectrum. Bands 1 through 4 and band 8 correspond to separate intervals of visible light and band 5 measures the near infrared (NIR) part of the spectrum (Figure 2.3). Bands 6 and 7 and 9 cover different sections of the short wave infrared (SWIR) light, while bands 10 and 11 corresponds to the thermal infrared (TIR) part of the spectrum (Figure 2.3).

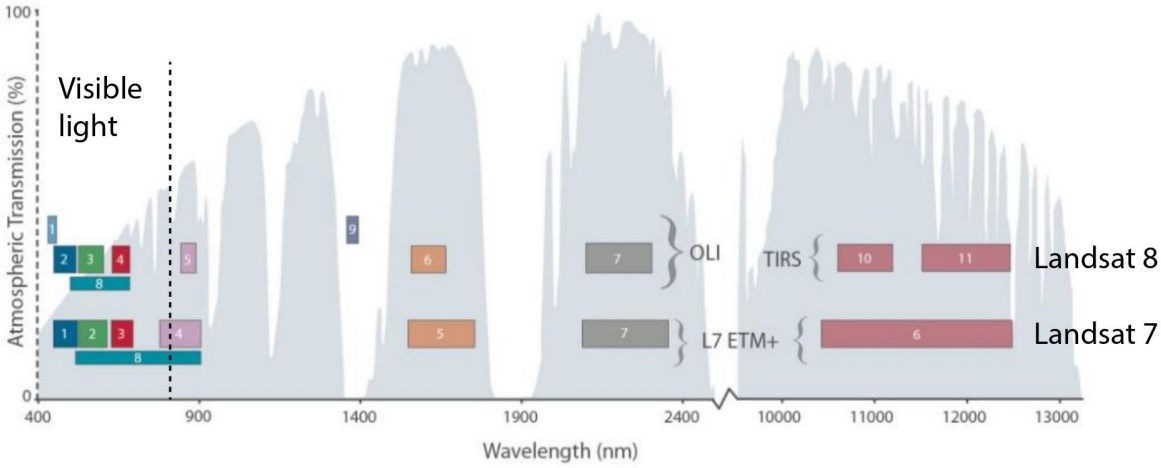

Figure 2.3 Illustration of what wavelengths the different Landsat 7 and Landsat 8 bands capture. Modified from NASA (2019).

The transmittance of light is defined as the ratio of light that is transmitted through an object to the total amount of light sent to the object (Jerlov, 1976). The properties of the material are affecting the transmittance factor, with reflection and absorption of wavelengths being the main controls on the total amount of light that is transmitted through the object. Transmittance of light

through the water column varies as a function of the wavelength (Pe'eri et al., 2014). It is typically light in the visible spectrum, wavelengths ranging from 350 nm to 700 nm, which can penetrate water to some extent. Light with a longer wavelength than 700 nm has low transmittance through water, as the water absorbs almost all radiation. This difference in water penetration is useful in satellite derived bathymetry, as the low transmittance of near-infrared and infrared wavelengths can be used to separate water from land. Also within the visible spectrum, the transmittance of light varies, with blue light being absorbed and scattered the most within the water column, while green light penetrates the water more easily. The relation between this difference in absorption of light between the blue and green values is used to estimate water depth (Pe'eri et al., 2014). The method of using satellite derived bathymetry is explained in Section 4.2.

3 GEOLOGICAL SETTING

This chapter will present the study area and put it in context with the large-scale geology of the surrounding area (Figures 3.1 and 3.3). The first part of this chapter looks at the regional context of on the Red Sea – Gulf of Aden rift system and its evolution. The second part focuses on the study area around the Sinai Peninsula, Gulf of Suez and Gulf of Aqaba and the environmental factors like climate, corals reef development and siliciclastic depositional style.

3.1 The Red Sea - Gulf of Aden Rift System

The Red Sea - Gulf of Aden rift system is a tectonically active area, part of the greater East African Rift System (Figure 3.1), which includes the Gulf of Suez, the Gulf of Aqaba and its basin margins (e.g. the Sinai Peninsula; Mckenzie et al., 1970; Bosworth et al., 2005). They link through the Afar triple junction, which is a rift-rift-rift triple junction, as the Red Sea, Gulf of Aden and Main Ethiopian rifts link (Figure 3.1). The Red Sea - Gulf of Aden Rift System separates the Arabian Plate in the north from the Nubian and Somalian Plates in the south, as the Arabian Plate is rotating counter clockwise away from Africa (Mckenzie et al., 1970; Le Pichon and Gaulier, 1988). A second triple junction is located on the northern Red Sea basin floor, just south of the Sinai Peninsula, where the Gulf of Suez and the Gulf of Aqaba link to the Red Sea (Courtillot et al., 1987). While the Red Sea and Gulf of Suez are rift basins, the strike-slip movement of the transform zone makes the Gulf of Aqaba a pull-apart basin (Garfunkel, 1981; Ben-Avraham, 1985). The transform fault in the Gulf of Aqaba is called the Aqaba-Levant transform (also known as the Dead Sea Rift) and is a sinistral strike-slip fault connecting the northern Red Sea to the convergence zone where the Eurasian and Arabian plates collide (Figure 3.1 Bosworth et al., 2005). This whole area has been extensively studied for decades, as this area is one of the first areas to be recognised as being a result of extension. Additionally it serves as a model for oceanic rifts and an example of an early stage (second stage) of the Wilson-cycle (e.g. a young oceanic basin; Wilson, 1969; Mckenzie et al., 1970).

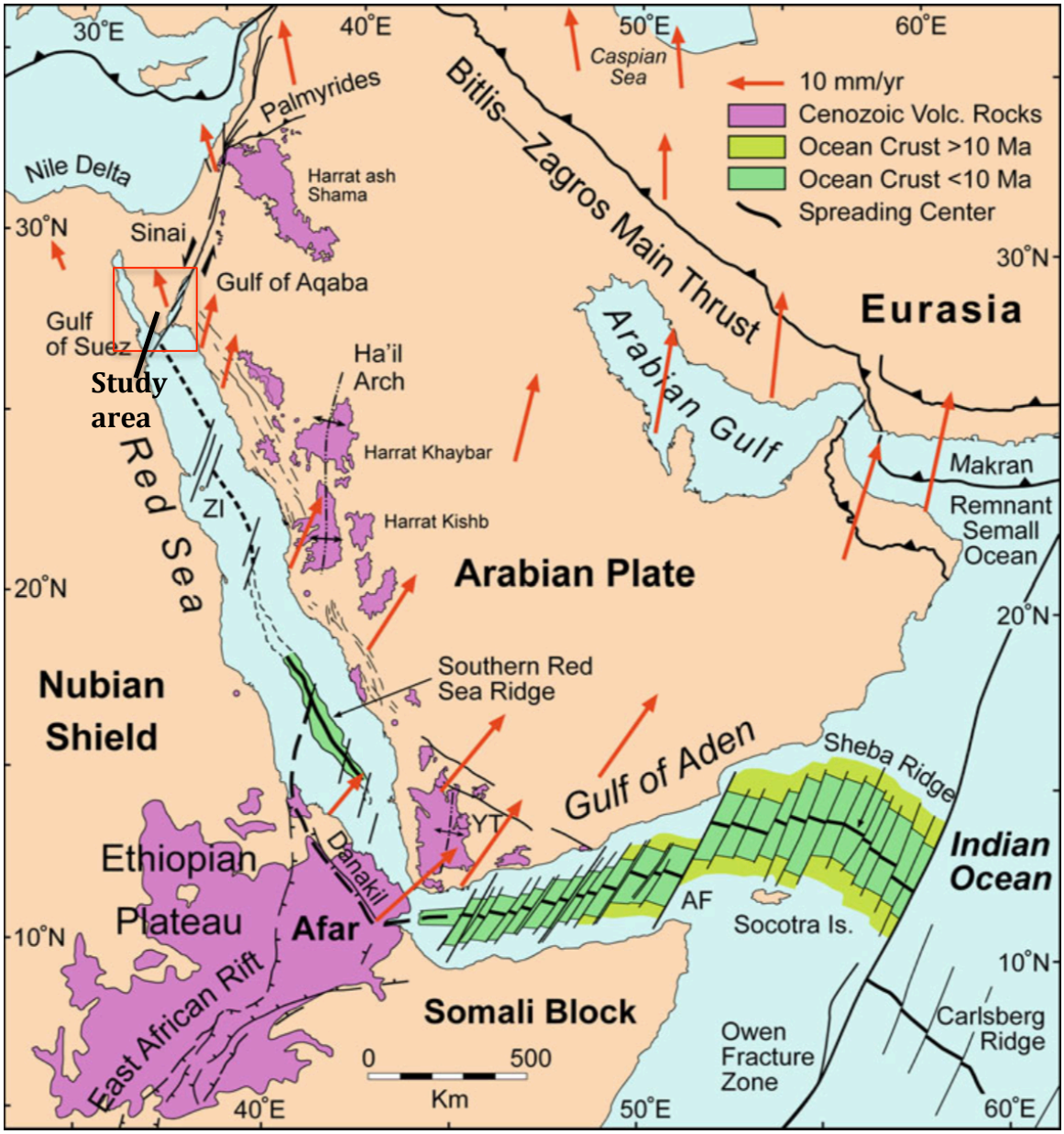

Figure 3.1 Structural map of the Red Sea – Gulf of Aden rift system. From Bosworth (2015)

3.1.1 Evolution of the Red Sea- Gulf of Aden Rift System

The first signs of rifting in this area dates back to early Oligocene at around 30-31 Ma. Extensive volcanism initiated in the Afar region, but little extension took place at this early stage (Figure 3.2a; Baker et al., 1996; Bosworth et al., 2005). However, in the few million years that followed, significant oblique rifting (NNE-SSW rifting to the ENE-WSW trend of the Gulf of Aden) took place in the Gulf of Aden and by the Oligocene-Miocene transition (~24 Ma) rifting spread throughout the Red Sea and to the Gulf of Suez (Figure 3.2b; Mckenzie et al., 1970; Steckler and ten Brink, 1986; Hughes et al., 1991; Manighetti et al., 1997).

During the Early Miocene the Gulf of Suez and Red Sea basins were one rift basin, structurally indistinguishable and depositionally linked (Figure 3.2b; Steckler and ten Brink, 1986; Bosworth et al., 1998). In the Middle Miocene a big structural event occurred, as the Arabian plate collided with the Eurasian plate: the initiation of the Aqaba-Levant transform fault, which connected to the Red Sea Rift at the Sinai triple junction (Figure 3.2c). This event separated the Gulf of Suez basin from the Red Sea and at the same time almost stopping the extension completely in the Gulf of Suez (Steckler and ten Brink, 1986; Bosworth, 1995; Bosworth et al., 1998). Furthermore, the onset of the Aqaba-Levant transform shifted the Red Sea rift motion from a normal rift movement to an oblique rifting, from ENE-WSW to NNE-SSW (Figure 3.2c; Steckler and ten Brink, 1986; Le Pichon and Gaulier, 1988; Bosworth et al., 2005).

During the Middle to Late Miocene the rift system transformed from a continental rift to the early stage of an oceanic rift, as spreading ridges propagated from the Indian Ocean into the Gulf of Aden (Mckenzie et al., 1970; Manighetti et al., 1997). Oceanic spreading in the Gulf of Aden initiated at 18-19 Ma (Sahota, 1991; Leroy et al., 2004). In the Red Sea, oceanic spreading started in the southern parts at 4-5 Ma and has propagated northward to the central areas of the Red Sea (Figure 3.2d; Cochran, 1983; Sahota, 1991; Bosworth et al., 2005). Today, the spreading ridges in the Red Sea and Gulf of Aden are not connected, but they are expected to connect through Afar in the future. Additionally the Red Sea spreading ridge is expected to continue propagating northwards and link with the Aqaba-Levant transform (Bosworth et al., 2005).

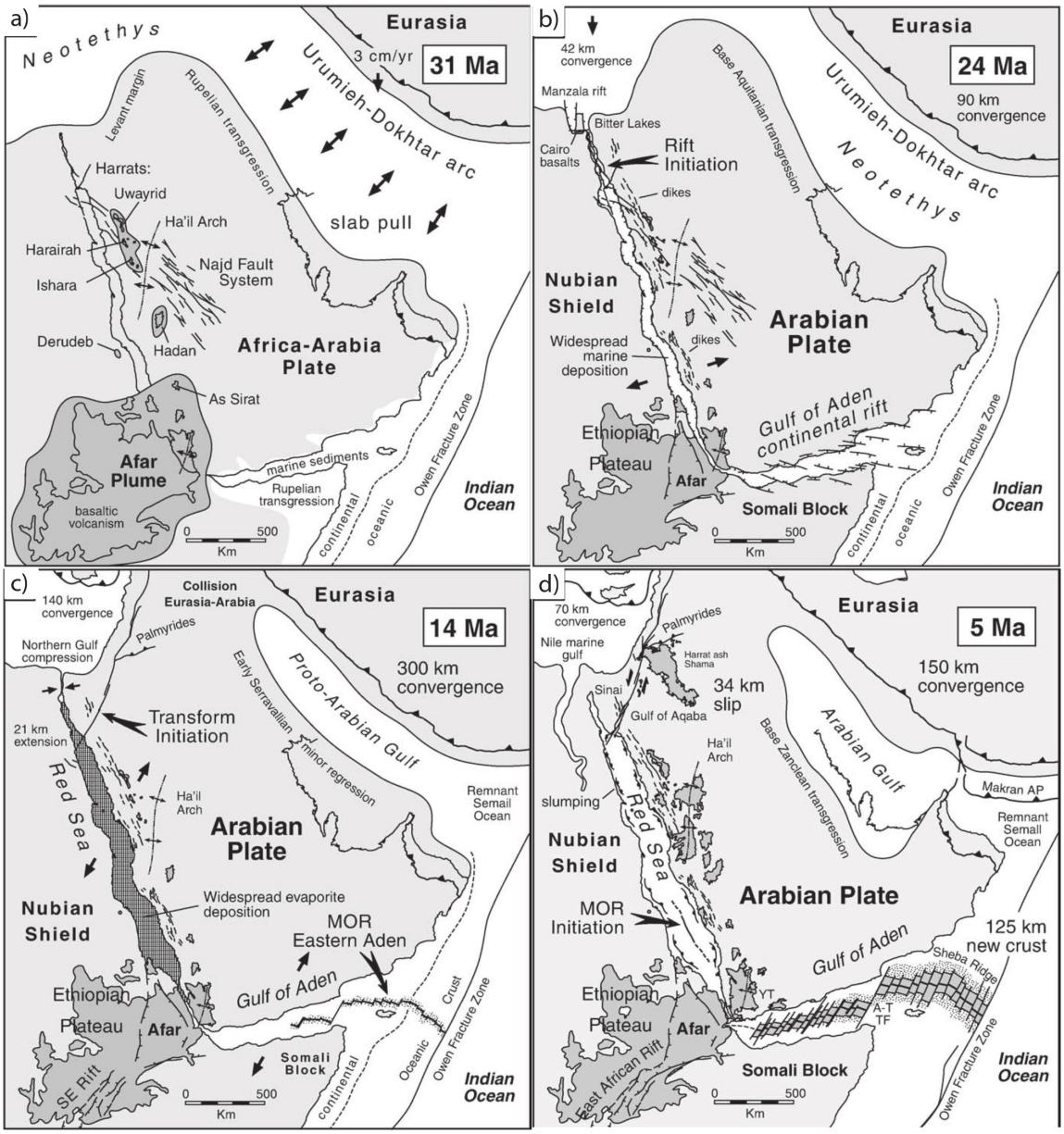

Figure 3.2 Illustration of the evolution of the Red-Sea – Gulf of Aden rift system. Modified from Bosworth et al. (2005).

3.2 Sinai Peninsula

The study area corresponds to the southern part of the Sinai Peninsula and the mid to southern parts of the Gulf of Suez and Gulf of Aqaba (Figure 3.3). This area consists of mountains reaching over 2500 metres in the central parts of the Peninsula with steep mountainsides going down to the Gulf of Suez and Gulf of Aqaba. A large percentage of the land area contains crystalline basement (Figure 3.4; Eyal et al., 1981; Sharp et al., 2000). The high relief is product of uplift due to

rotating fault blocks in the Gulf of Suez. Throughout Sinai magmatic dikes of numerous ages can be found, the earliest being of the Precambrian age, but most of them are related to the African-Arabian rifting event (Eyal et al., 1981).

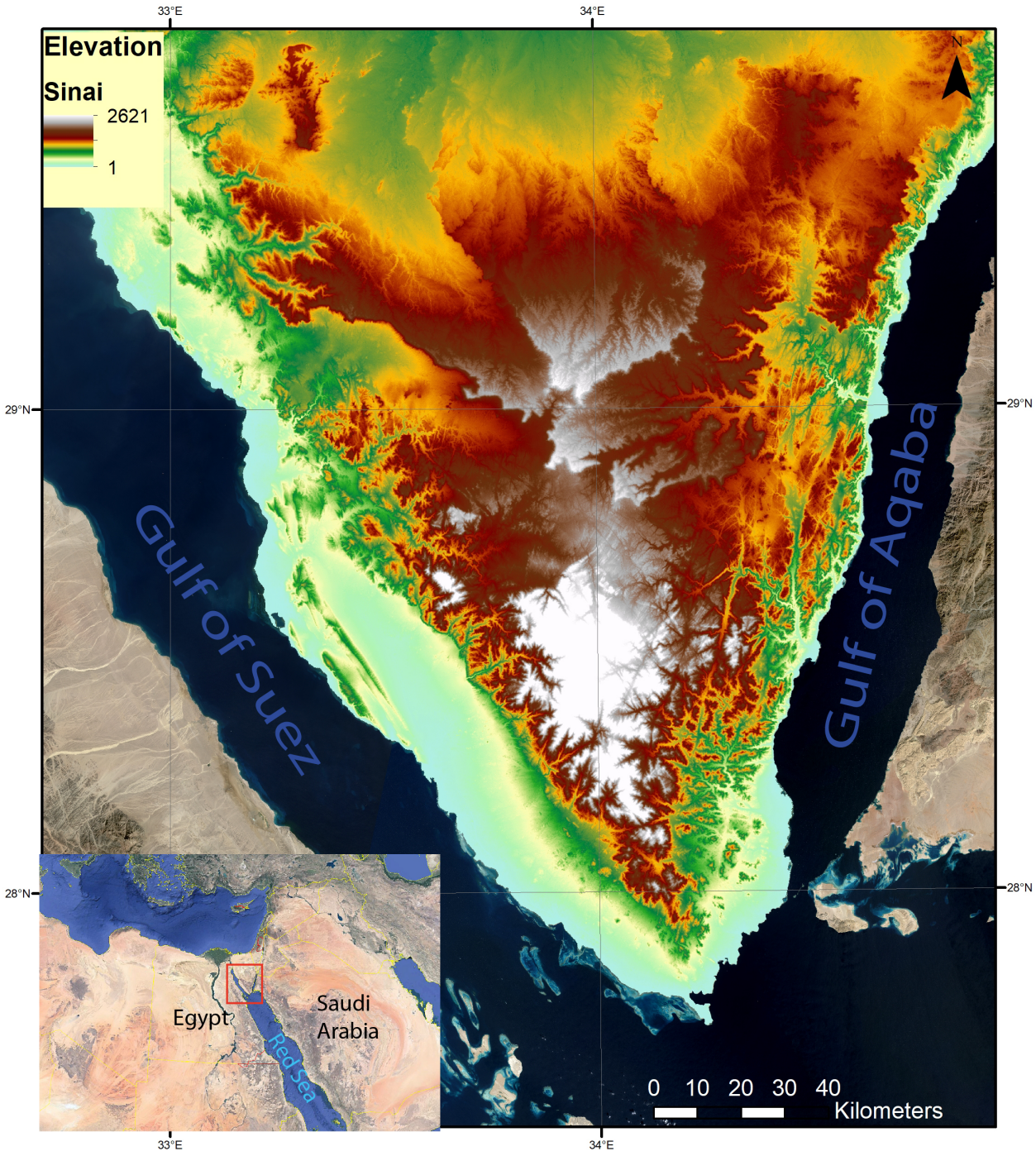

Figure 3.3 Elevation map for the Southern Sinai Peninsula

3.2.1 Gulf of Suez

The Gulf of Suez is an elongated, abandoned rift basin, approximately 300 km long and 80 km at its widest. Currently the basin is considered a dead rift basin, as there is minimal rifting activity. The large basin-bounding normal faults are parallel to the gulf, trending NNW-SSE. Large transfer zones, creating a zigzag pattern, link these faults (Figure 3.4; Gawthorpe and Hurst, 1993). The Gulf of Suez can be divided into three provinces of asymmetric dip, separated by transfer zones, with hanging walls dipping in different directions (Figure 3.4). In the southernmost part of the Gulf of Suez the hanging wall dips towards SW, while the main dip direction is towards NE in the central parts. In the northern area, the dip direction is again towards SW (Figure 3.4; Gawthorpe and Hurst, 1993; Sharp et al., 2000; Khalil and McClay, 2002). The study area includes the two southern dip domains (Figure 3.4).

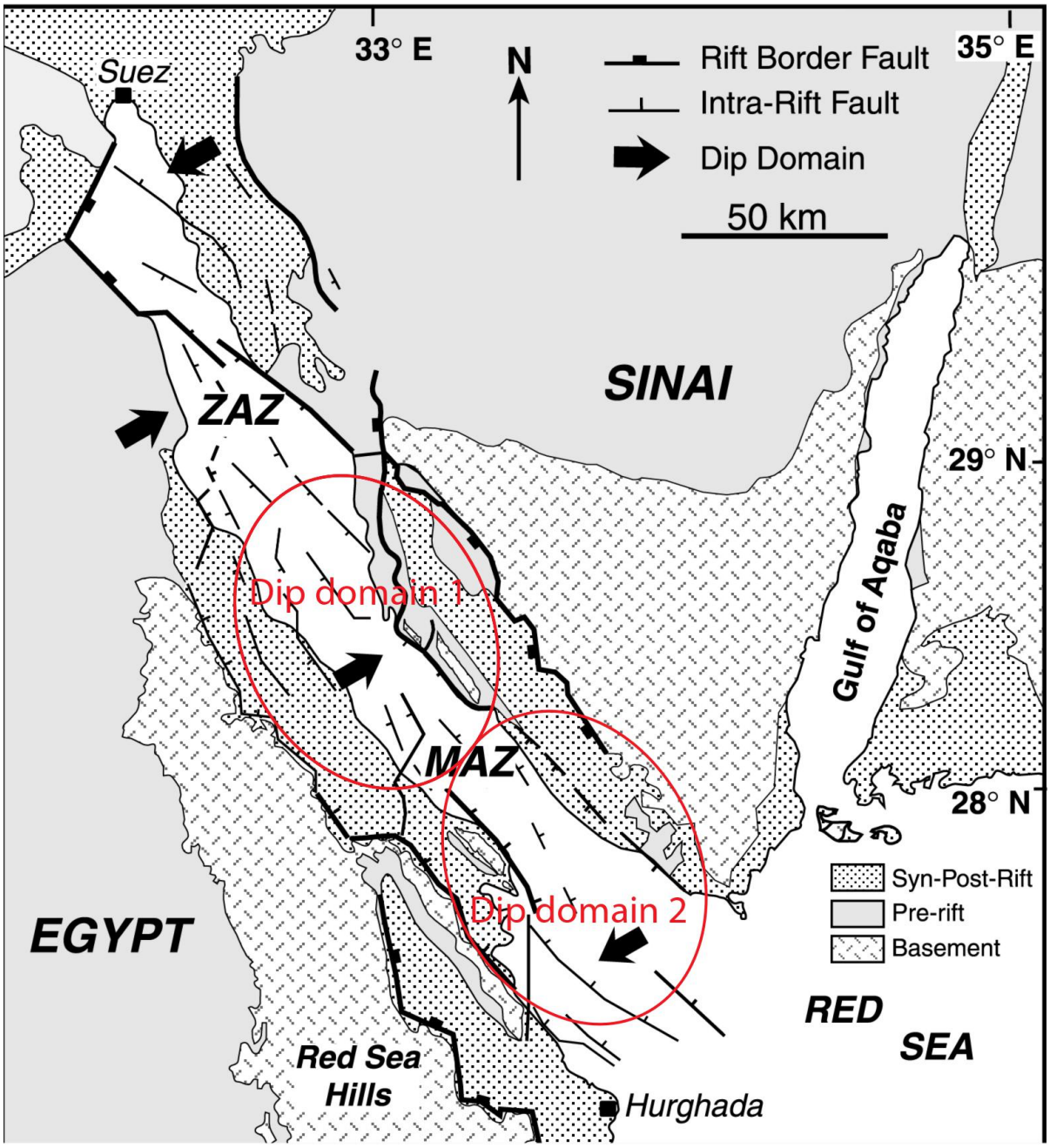

Figure 3.4 Geological map of the Sinai Peninsula, showing the main structures of the Suez rift basin. ZAZ and MAZ are the Zaafarana and Morgan Accomodation Zones, and represents the major transfer zones in the gulf. Two dip domains are found within the study area (red circles). In Dip donain 1 the Sinai coast is characterised by footwall scarp fan deltas, while in Dip domain 2 latteraly more extensive hanging-wall fan deltas develop. Modified from Khalil and McClay (2002)

3.2.2 Gulf of Aqaba

The Gulf of Aqaba is an elongated pull-apart basin, approximately 180 km long and 30-40 km wide. The Gulf of Aqaba is the southernmost part of the Dead Sea rift structure, which is a 1100 km sinistral strike-slip fault system, connected to the northern Red Sea in the south and extends to the Taurus mountains in Turkey in the north (Eyal et al., 1981; Ben-Avraham, 1985). This basin is a result of several strike slip faults overlapping and linking through transfer zones, where the crust is thorn apart obliquely (Figure 4.4; Ben-Avraham, 1985). The Gulf of Aqaba is the result of several smaller pull-apart basins, and the nature of these structures is the reason the basin reaches depths of more than 1300 m in several areas, with the deepest parts reaching depths of approximately 1800 m (Ben-Avraham, 1985).

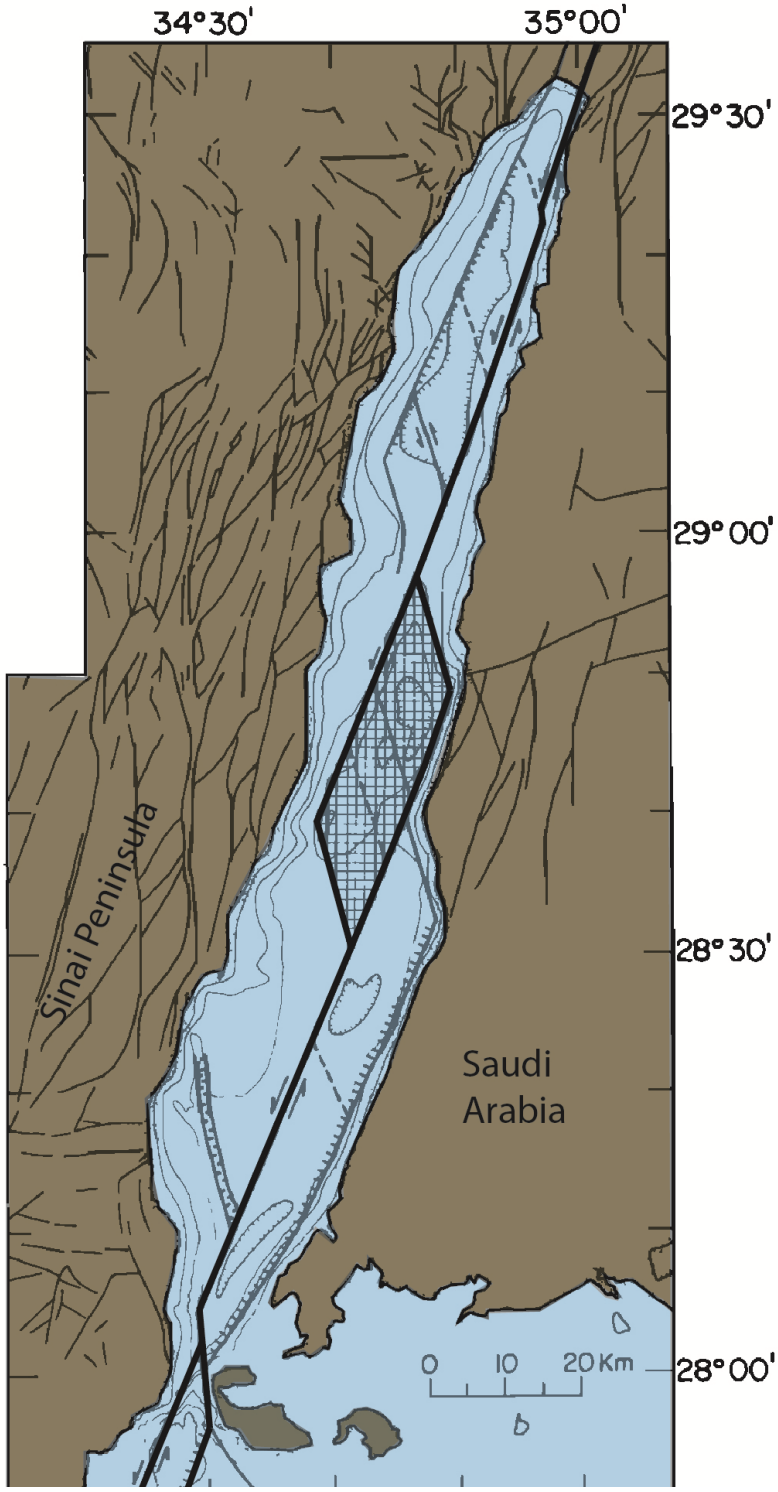

Figure 3.5 Depicts overlapping strike-slip faults, resulting in pull-apart basin in the transfer zone. Modified from Ben-Avraham (1985).

3.2.3 Climate

The Sinai Peninsula is located in a hyper-arid area, where high temperatures and low precipitation rates are the dominant conditions throughout the year. The rain that does fall typically occurs during the winter months. The distribution of precipitation is controlled by topography, with most of the rain falling in high elevated regions of the peninsula (Issar and Gilad, 1982). The coastal areas rarely get more than 15 mm of annual rainfall (Hermas et al., 2010). During exceptional years, the yearly rainfall can manyfold, with most of the additional precipitation occurring within a short time span (days or weeks) (Issar and Gilad, 1982).

Extreme rainfall in a short period of time can cause flash floods throughout the Sinai Peninsula, which has the possibility to cause severe damage to people and man-made structures. The typical flash flood occurs once every few years, only affecting the high lying areas, and does not reach the alluvial fans and the coastal areas. Only in extreme cases does the flash floods reach the coastal fan deltas, transporting sediments and debris to the coastal area (Issar and Gilad, 1982).

In addition to dry and hot weather conditions, strong winds blow from the north along the strike of Gulf of Suez and Gulf of Aqaba (Nir, 1996). The high speeds of the winds are caused by the high mountains on each side of both gulfs, channelling the winds through the gulfs (Roberts and Murray, 1984; Purkis et al., 2015). These winds, are unidirectional and always blowing southward, with the exception of only 3 % being winds form the south (Roberts and Murray, 1984). As a result of these winds, there is a main southward trend of longshore sediment transport along both gulfs, and are especially visible where sediment accumulate on the northern parts of man made structures (Figure 3.6; Nir, 1996).

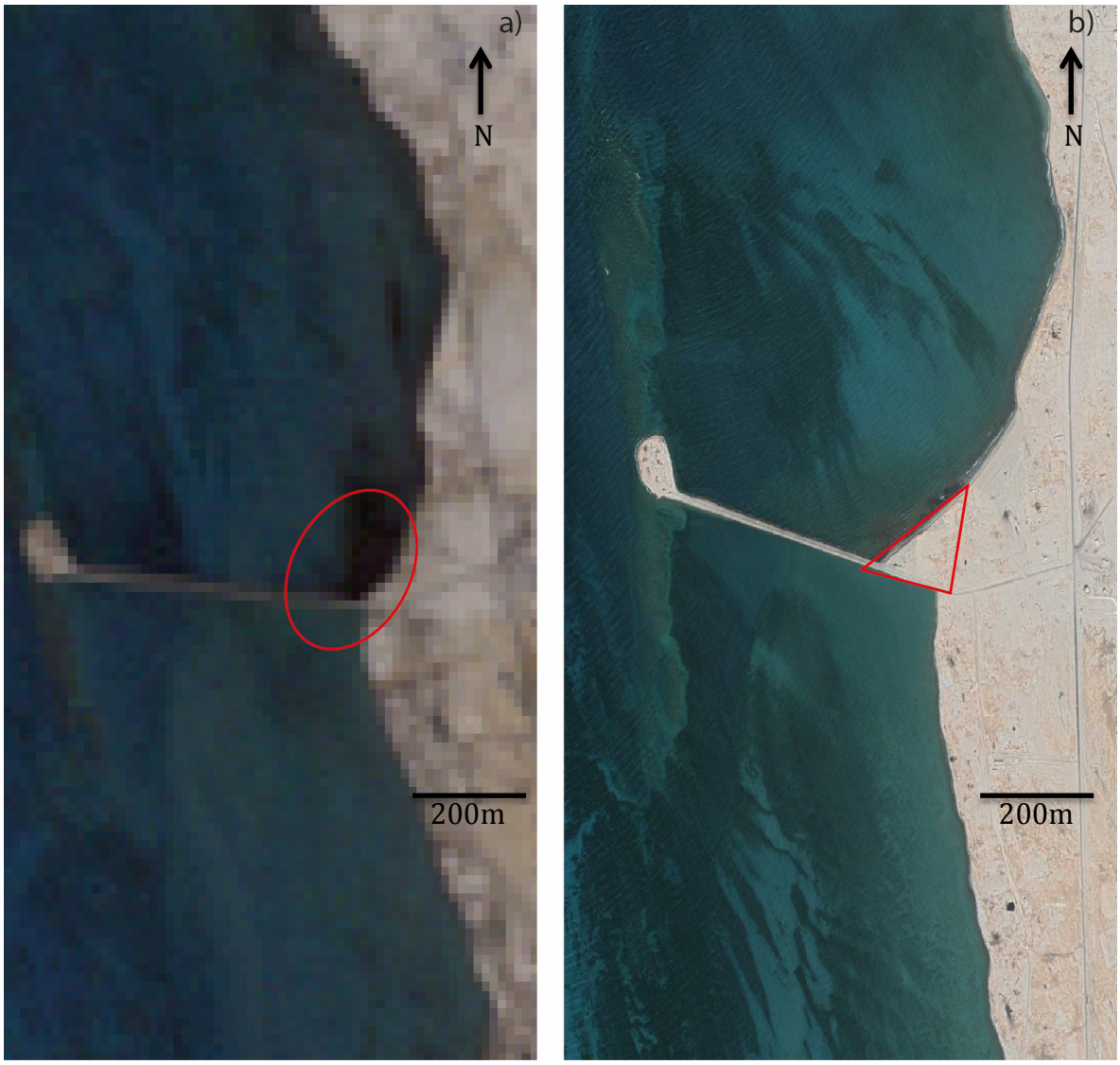

Figure 3.6 a) Landsat satellite image from 1988 and b) Google Earth image from 2019 of a structure in the Gulf of Suez. Sediments have accumulated on the northern side of the structure, indicating longshore drift going north to south.

It is also relevant to note that even though climate is arid today, there have been periods as recent as early and mid Holocene, where the climate was more humid, with greater rainfall (Purkis et al., 2015; Rowlands and Purkis, 2015). During these wetter climate conditions the sedimentation rate and the rate of progradation on the coastal fan deltas was higher. Sea-level changes during the Quaternary glaciations have had an effect on depositional environments (Purkis et al., 2015). Coastal fan deltas prograded and reached further during glaciations

and low sea level, while retrograding during interglacial periods. During glacial maximums, like Last Glacial Maximum, the whole Gulf of Suez dried out as sea-level dropped ~120 m, well below the 70 m average bathymetry of the gulf (Nir, 1996; Dullo and Montaggioni, 1998). Conditions for the present day coral reefs became optimal after the last glaciation as sea level started to rise. The corals spread, developed and climbed with the rising sea level, until it stabilised around 6500 years ago (Nir, 1996).

3.4 Coastal fan deltas

Both Gulf of Suez and Gulf of Aqaba have a narrow coastal zone (1-10 km) at the base of the high and steep mountains of central Sinai (e.g. Purser et al., 1987; Roberts, 1987; Dullo and Montaggioni, 1998). The steep mountainsides combined with infrequent, but severe flash flood events transport coarse, unsorted sediments to the coastal areas, developing alluvial fans and fan deltas along the entire coast of the Sinai Peninsula (e.g. Roberts, 1987; Bosence, 2005). The arid climate of this area results in high evaporation rates, which creates sabkha environments on the low-relief, most distal parts on the coastal fans, depositing halite, gypsum and anhydrite (Purser et al., 1987; Roberts, 1987).

Within the study area the Gulf of Suez can be divided into two distinct dip domains (Figure 3.6). Dip domain 1 is the central part of the Gulf of Suez and has a hanging-wall dip towards the NE, while dip domain 2 is the southern Gulf of Suez, which has a dip domain of SW (Gawthorpe and Hurst, 1993; Sharp et al., 2000; Khalil and McClay, 2002). This favours development coarse-grained fans adjacent to the footwall scarp in dip domain 1, while laterally more extensive hanging-wall fan deltas develop along coast of dip domain 2 (Figure 3.6; Gawthorpe and Colella, 1990).

3.5 Coral Reefs in Gulf of Suez and Gulf of Aqaba

Coral reefs and carbonate production is found throughout the Red Sea and its two northern gulfs (e.g. Hayward, 1982; Nir, 1996; Dullo and Montaggioni, 1998; Rowlands et al., 2014). In the Gulf of Suez and Gulf of Aqaba corals are mainly of the fringing reef type (Nir, 1996; Dullo and Montaggioni, 1998). Fringing reefs

form a narrow band along the coast and are of the attached type, only separated from the coast by a narrow water area. Corals in the Gulf of Aqaba are almost only of the fringing type, with the reefs almost attached directly on the coast due to the steep morphology of the basin (Dullo and Montaggioni, 1998). Due to the shallow nature of the Gulf of Suez, more corals can develop in this basin, with barrier reefs and detached platforms also developing, especially in the southern part of the gulf (Nir, 1996; Dullo and Montaggioni, 1998).

Scleractinian corals, organisms that build hard skeletons, are the most important reef building organism in the fringing reefs in the Red Sea area (Hayward, 1982; Dullo and Montaggioni, 1998). The *Stylophora* is the most common organism in fringing reefs and make up ~20 % of these reefs (Hayward, 1982). Another important frame-building organism is the *Millepora* (Hayward, 1982; Dullo and Montaggioni, 1998). Furthermore, a diverse fauna, including molluscs, red algae, seagrass and other scleractinian corals, make up the remaining parts of the reefs in the Red Sea, Gulf of Aqaba and Gulf of Suez (Hayward, 1982; Dullo and Montaggioni, 1998)

Bosence (2005) classified corals based on basinal and tectonic setting and identified three features important for coral reef development in the Red Sea: 1) fault block, 2) delta-top and 3) salt diapir (Figure 3.7). The delta-top type occurs where the accumulation of terrestrial sediments creates topographic highs in the coastal zone (Bosence, 2005; Rowlands et al., 2014). When the alluvial fans are undisturbed from siliciclastic sediments for a long enough time, corals start to colonise the shallow-water areas on the fans (Figure 3.7a; Rowlands et al., 2014). The fault block type is caused by the rotation of fault blocks as rifting takes place, creating topographic highs on the basin floor where corals can colonise (Figure 3.7b). The movement of evaporites in the subsurface causes salt diapirs. The evaporites are less dense, and tend to rise up and distort surrounding rock, causing bathymetric highs where corals can occupy (Figure 3.7c; Bosence, 2005; Rowlands et al., 2014).

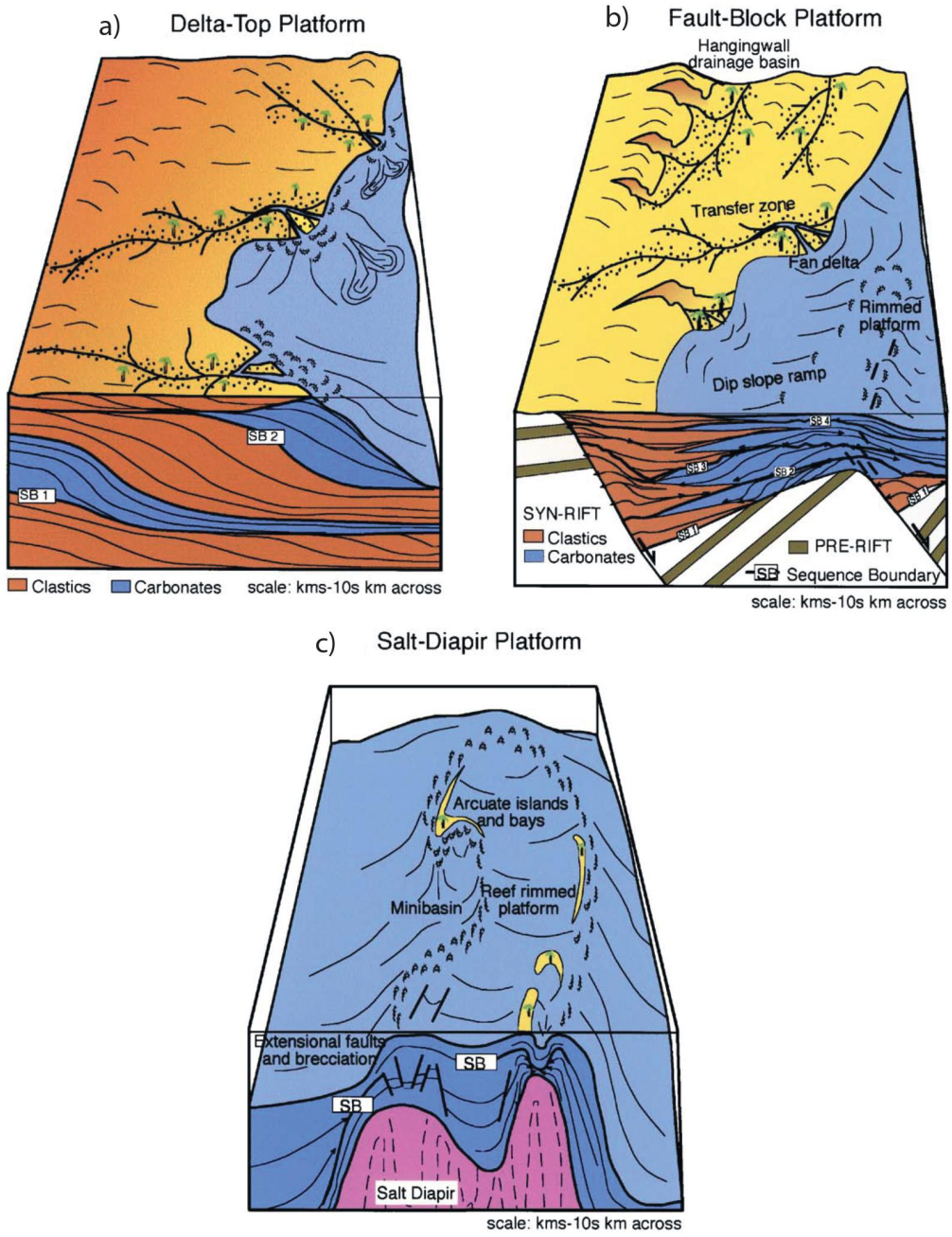

Figure 3.7 Three tectonic settings important for coral reef growth in the Red Sea, Gulf of Suez and Gulf of Aqaba. From Bosence (2005)

In the Gulf of Suez, the delta-top and fault block types are the main reason for the development of coral reefs (Roberts, 1987; Dullo and Montaggioni, 1998; Bosence, 2005). Salt diapirs however, are not a common feature in the gulf, but can be found in the southernmost part (Bosence, 2005). The basin configuration

of the Gulf of Aqaba makes it so that the delta-top type is the only way that corals can develop in the basin (Bosence, 2005).

3.5.1 Siliciclastic influence

The delta-top setting is the most important element for coral reef growth in the Sinai area, but it is also the most vulnerable to terrestrial siliciclastic input (Bosence, 2005). As coral reefs are sensitive to siliciclastic input, the occasional heavy rainfall and flash flood event can be desruptive to the coral reefs (Hay et al., 1988; Bosence, 2005; Rowlands and Purkis, 2015). Both along the Gulf of Suez and Gulf of Aqaba, alluvial fans are dominating the coastal sedimentary environment. The band of corals along the coasts are usually only interupted at the mouth of active distributary channels on the alluvial fans (Roberts, 1987; Dullo and Montaggioni, 1998). Ephemeral rivers drain the mountains, only transporting water and sediment to the alluvial fans during flash flood events (Rowlands and Purkis, 2015). During extreme flash flood events, corals may be temporarily destroyed as sediment scour through the carbonate environment (Dullo and Montaggioni, 1998; Rowlands et al., 2014). However, the warm, dry and stable weather conditions of the Sinai Peninsula can last for 10s to 100s of years without any major or severe event (Dullo and Montaggioni, 1998; Rowlands and Purkis, 2015). This results in favourable conditions for coral growth and carbonate production (Roberts, 1987). The coarse-grained alluvial fans are considered to be important features for coral development on delta-tops (Purser et al., 1987; Bosence, 2005). The sporadic nature of siliciclastic input creates an environment where corals and clastics can coexist, with rapid transitions from carbonate to siliciclastic deposits (Purser et al., 1987; Bosence, 2005).

4 METHODS AND DATA

This chapter explains what data and methods were used to conduct the analysis in this study and describes the workflow behind the methods. This study combines the use of digital elevation models (DEM) and Landsat satellite imagery (30 m spatial resolution) to investigate the drainage pattern, the development of coastal fan deltas and the shallow-water (down to 5m depth) environment of the southern Sinai Peninsula. Satellite imagery was used to derive the shallow water bathymetry (Satellite Derived Bathymetry).

4.1 Digital extraction

An ArcGIS analysis of the modern geomorphology and drainage pattern was conducted of the southern parts of the Sinai Peninsula using a Digital Elevation Model (DEM). Satellite imagery was used to map and digitise the coastal fan deltas. Workflow using the DEM is shown on Figure 4.1.

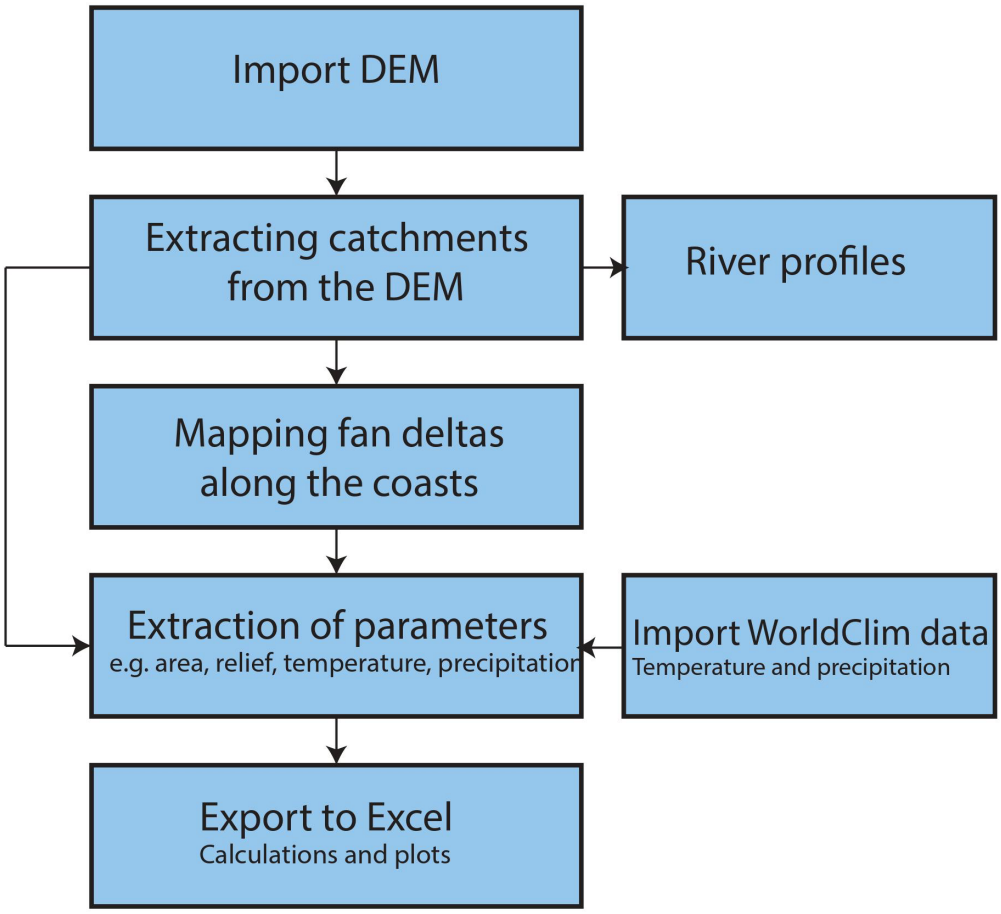

Figure 4.1 Flowchart of the work using DEM to extract geomorphological data of the Sinai Peninsula

4.1.1 Data and software

This thesis uses ASTER Global Digital Elevation Model (cell size: ~30x30m), downloaded from NASA´s EarthDATA webpage, as it is publicly and freely available (NASA, 2009). A Digital Elevation Model (DEM) is a raster dataset containing digital elevation data. A DEM is the representation of a topographic surface with each cell representing the elevation at its location. The DEM was processed and analysed using ESRI's ArcGIS software. Using ArcGIS tools it was possible to extract features for geomorphological analysis from the DEM, such as elevation information, drainage areas, drainage networks and profiles. In this study the *Spatial Analyst*, *3D Analyst* and *Data Management* toolboxes were the most frequently used for the extraction and analysis. The main analysis was performed with the *Hydrology* tools within the *Spatial Analyst* toolbox, extracting flow patterns, drainage networks and watersheds. From the extracted drainage network, *3D Analyst* tools and *3D Analyst* toolbar were used to obtain the river profiles.

4.1.2 Analysis of catchment areas

Catchment areas were extracted from the DEM of the Sinai Peninsula. The DEM was originally in a geographic coordinate system (WGS 1984) and was therefore projected to Universal Transverse Mercator coordinate for the specific area (UTM 36N). The first three steps of the processing, in order to extract drainage areas from the DEM, were to determine the accumulation of each cell, which creates a raster simulating how water flows in the DEM. These steps include filling sinks in the DEM, creating a flow direction array and a flow accumulation array. Sinks are depressions in the DEM, often caused by errors in the data set (Tarboton et al., 1991), which can artificially trap water during processing and produce a discontinuous drainage network. From the resulting flow accumulation array, and using satellite images as guidance, a point feature class containing interpreted apex points was created. Based on these points and the flow accumulation data, polygons were extracted, which represents the catchment areas (Figure 4.2). Catchment areas and fan deltas are together referred to as drainage systems, and the systems are numbered from 1 to 20

going anticlockwise around the Sinai Peninsula starting from the northern part of the Gulf of Suez (Figure 4.2).

Figure 4.2 Drainage systems (catchments + fan deltas) mapped in the Sinai Peninsula indicated with numbers. Square indicates the location of figure 4.2.

4.1.3 River profiles

River profiles were extracted from each of the catchments, extending from sea level and to the highest point within each catchment. Longitudinal profiles were extracted from the longest river within each drainage area. To extract the profiles the accumulation raster had to be converted into polylines in a feature class. The desired polylines were selected within a catchment to create the longitudinal river profile.

4.1.4 Fan mapping

Fan deltas were mapped in ArcGIS guided by Landsat 8 satellite imagery and the extracted catchment delineations (Figure 4.2). Polygons were manually drawn to represent the surface area of the coastal fan deltas along the Sinai coasts. In the southern part of the study area, especially on the Gulf of Suez, the fan deltas coalesced in laterally amalgamated fan deltas where it was hard to distinguish the fans from one another. In this area the fans were drawn so that each of the extracted catchment areas are associated with one fan delta (Figure 4.2). However, drainage system 4 has 7 catchments (4a through to 4g) all draining into the same fan (Figure 4.3).

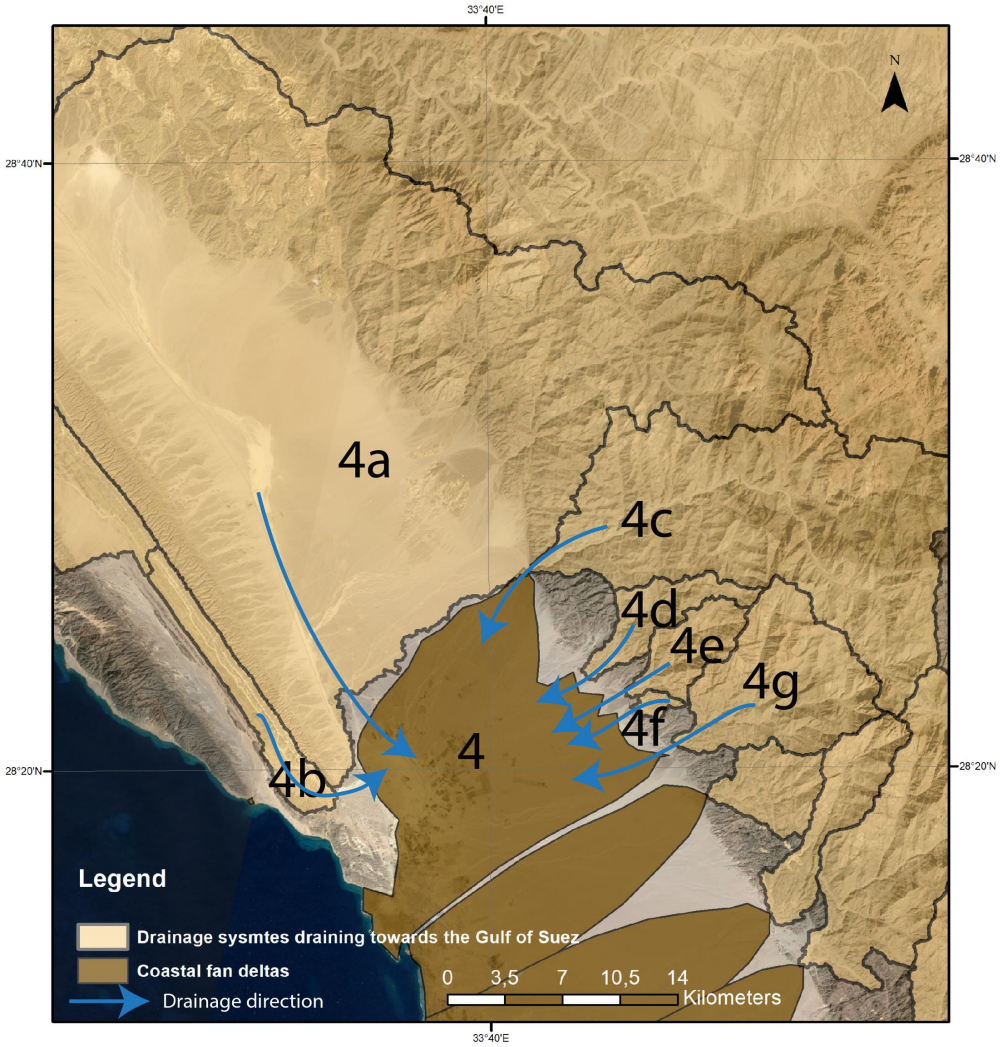

Figure 4.3 Drainage system 4 contains 7 catchments draining into the same fan delta.

4.1.5 Temperature and precipitation

Average temperature and precipitation values for each catchment area was derived from the Global WorldClim 2 dataset (Fick and Hijmans, 2017). This worldwide data presents climate parameters, such as temperature and precipitation, and contains monthly averages for the years 1970-2000, at a ~1km^2 spatial resolution. For each of the 12 months of data, both for temperature and precipitation, the data was projected to UTM 36N coordinates. The data was then cropped to include only the study area. Precipitation and temperature data was extracted for each catchment area, and exported to Excel. To calculate the yearly average temperature, the monthly average values were added together and then divided by 12. The annual precipitation was calculated by simply adding together the 12 monthly averages.

4.2 Satellite Derived Bathymetry

Landsat satellite images and depth soundings from nautical charts were used to derive shallow water bathymetry down to 5 m depth. Figure 4.4 shows the workflow for deriving the bathymetry from Landsat satellite images. This section explains satellite derived bathymetry using Landsat 8 satellite images.

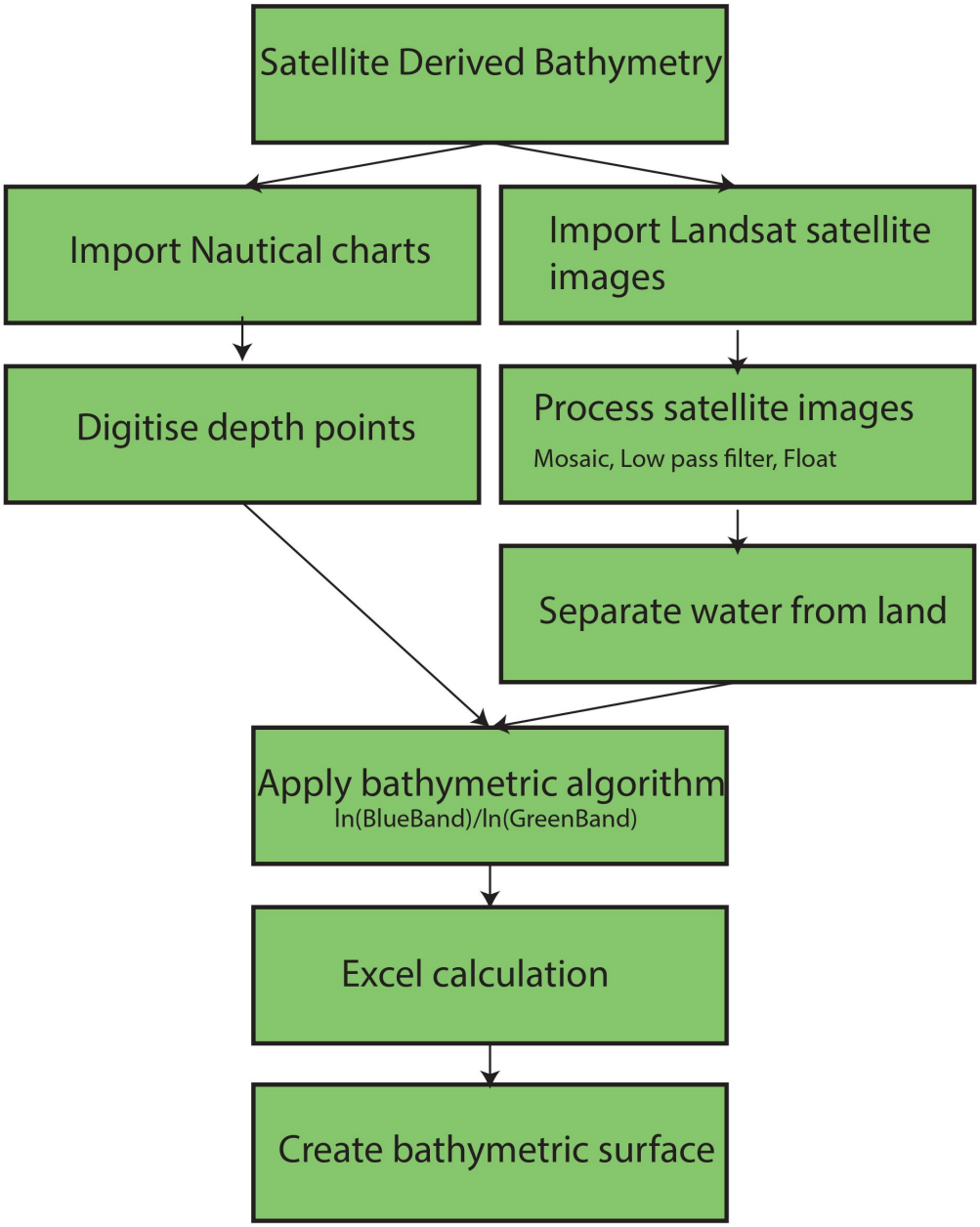

Figure 4.4 Flowchart showing the step-by-step process for deriving bathymetry from satellite images.

4.2.1 Nautical charts and depth soundings

Nautical charts

In order to create bathymetric models of the two marine basins, nautical charts were needed, as depth data from the charts were used as soundings in deriving bathymetry from satellite images. Two nautical charts in paper format covering the Gulf of Suez, delivered by the United Kingdom Hydrographic Office (UKHO), were used to acquire depth sounding. The two charts were scanned and digitised as JPEG files, which could then be used in ArcGIS.

Nautical chart of the Gulf of Aqaba was also from the UKHO, but from an online source (NOAA and UKHO, 2019). To create a chart that is useful in ArcGIS, around 30 screenshots were taken to cover the whole gulf. The screenshots were then mosaiced into one large image and exported as a JPEG file.

Both nautical charts had to be georeferenced in ArcGIS in order for them to be useful. Georeferencing is done in order for the charts be geographically correctly placed in the coordinate system. The points were chosen and placed on the coordinate grid where lines of longitude and latitude cross each other, as these are points on the chart that have known geographic coordinates.

Depth soundings

From the georeferenced nautical charts the depth points were manually selected and digitised. On contour lines on the nautical charts, several depth points were picked along the same contour in order to get as accurate results as possible. By doing this, around 58 000 depth points were digitised along the two gulfs, with values ranging from 0 to 1000 m. These digitised points were then used in deriving bathymetry from satellite images. In addition, the points were used to make an interpolated depth surface, using Natural Neighbours, of the study area as a reference surface.

4.2.2 Deriving bathymetry

The process of deriving a bathymetric model from the Landsat 8 satellite images is described in detail below. The workflow used in this study was based on the workflow outlined by the International Hydrographic Organization and Intergovernmental Oceanographic Commission in Chapter 14 of the IHO-IOC GEBCO Cook Book (2018). The principles for extracting a bathymetric model from multispectral satellite imagery are provided by Pe'eri et al. (2014) and Stumpf et al. (2003).

To derive bathymetry from Landsat 8 satellite images, bands 2 (450-515 nm), 3 (525-600 nm) and 6 (1560-1660 nm) were used. Bands 2 and 3 are used to calculate the bathymetry and band 6 is used to separate water from land. Mosaic was created of each of the bands 2, 3 and 6 to cover the entire study area.

The next step is to separate land and water, so that only the marine areas are displayed for each band. This is possible to do using band 6, as infrared radiation is absorbed by water. A profile across both water and land from band 6 was drawn (Figure 4.5). In band 6, low pixel values represents water areas and high, fluctuation values represent land areas. This difference makes it possible to identify a threshold pixel value between water and land. The threshold value was used to extract only the water areas on bands 2 and 3 (Figure 4.7b). A low pass filter in ArcGIS was used on

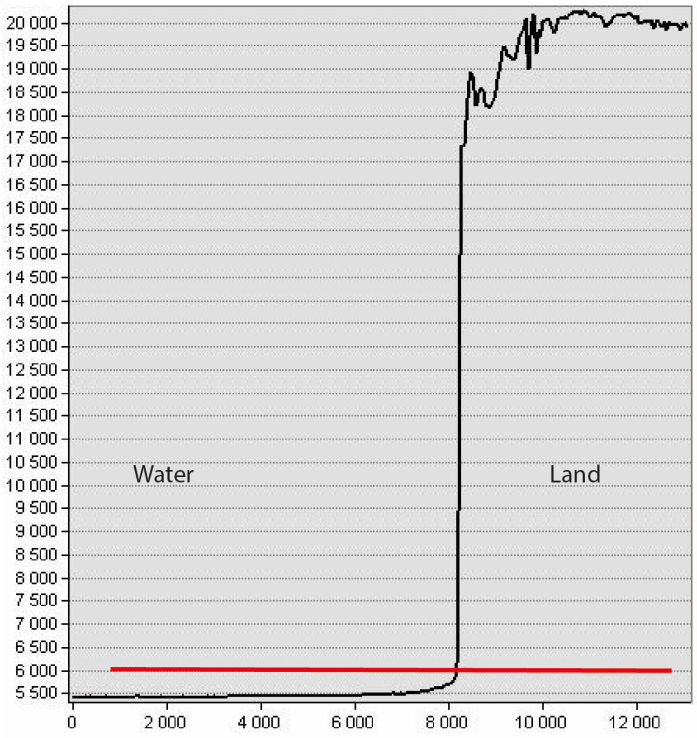

Figure 4.5 Values measured for band 6 (1560-1660 nm) along a line drawn on the satellite image that contains both a seawater and a land section. The threshold value separating land from water is 6000 in this example. X-axis is the distance across the profile; Y-axis is pixel-values of band 6.

the bands as Pe'eri et al. (2014) found that applying a low pass filter provides more accurate results.

The next step was to apply the bathymetry algorithm to the depth points extracted from the nautical charts. From band 2 and 3, containing only the water areas, a surface using the equation ln(band2)/ln(band3) was calculated. This equation is referred to as the bathymetry algorithm. Each depth sounding digitised from the nautical charts got assigned a value from the bathymetry algorithm. Depth points that have the same depth value might have slightly different algorithm values, so an average algorithm value was calculated for each unique depth value. A scatter plot was then created from these values (Figure 4.6a) and only the depth points that showed a more or less a linear trend (8-9 m in this example) were chosen for a second scatterplot, to which a trend line was calculated (Figure 4.6b). The resulting trend line was used to calculate and create a bathymetric surface in ArcGIS of both gulfs (Figure 4.7c). Values deeper than 5 m matched poorly with the reference surface and the nautical charts. A new bathymetry surface was therefore created to only include the shallow-water bathymetry down to 5 m depth (Figure 4.7d). Limitations to satellite derived bathymetry is discussed in section 6.5.

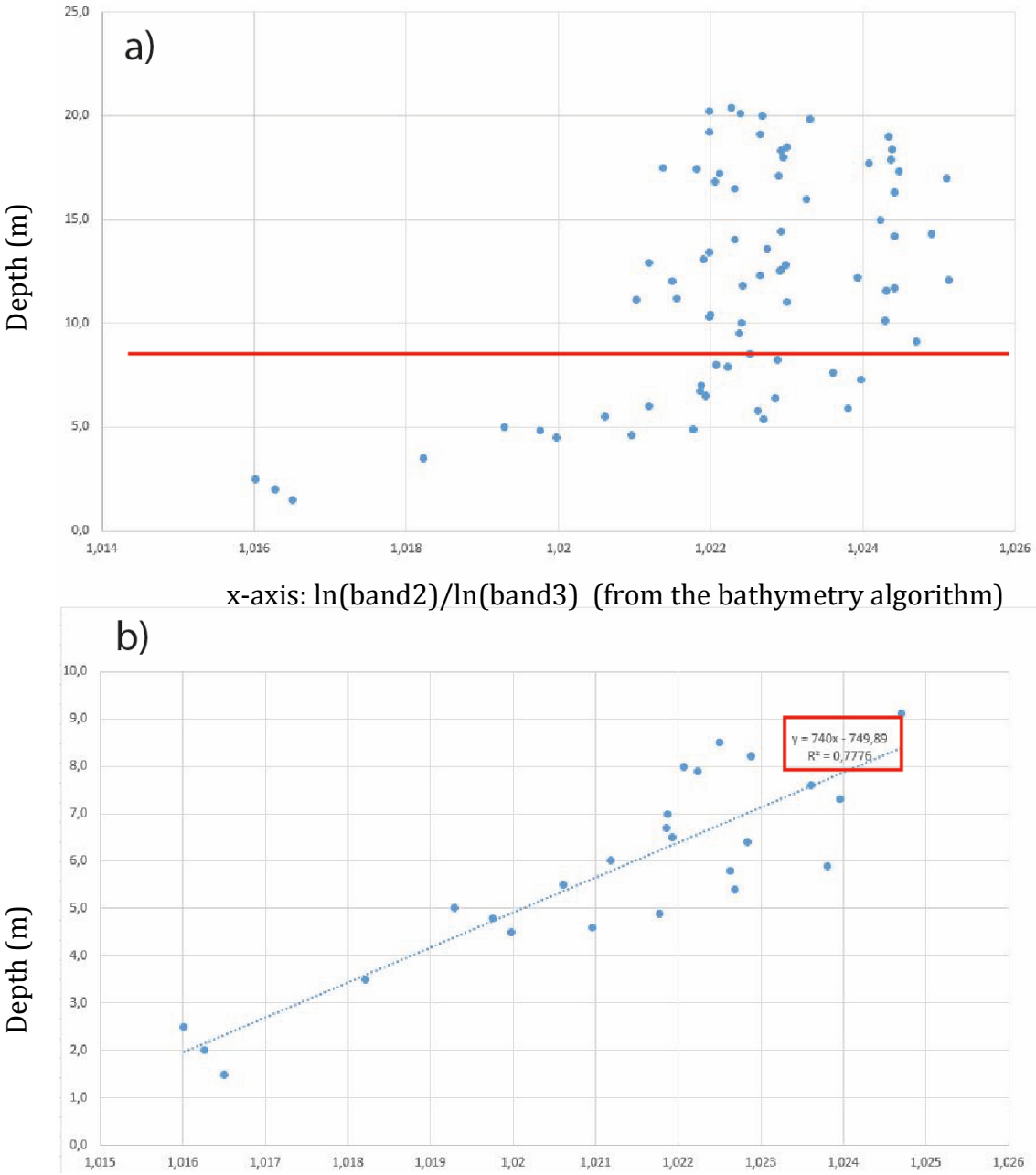

Figure 4.7 Scatterplots showing the relation between depth and values of from the algorithm (ln(band2)/ln(band3)). a) Scatterplot with values up to approximately 20 m depth. The data shows a linear trend up to the threshold (red line) with no clear trend for the data lying above that threshold. b) Scatterplot for the data lying below the threshold in a). The equation for the trend line is used as input in calculating the bathymetry.

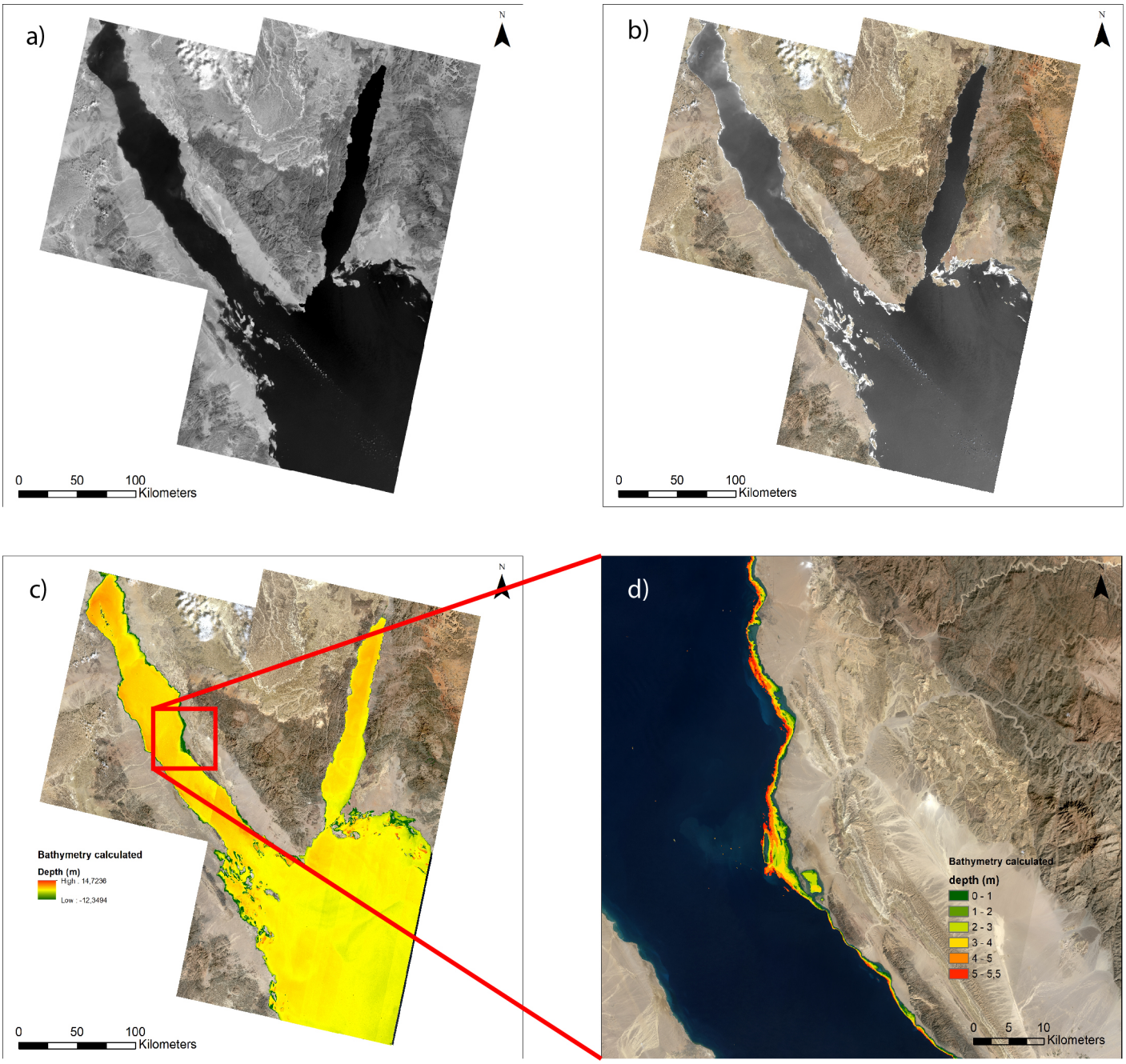

Figure 4.8 Illustrating some of the steps for deriving the shallow-water bathymetry, from Landsat 8 satellite imagery, down to 5 m depth. a) Band 2 covering the entire study area. b) Illustrates water bodies separated from land. c) The calculated bathymetry from the equation calculated in Excel. d) Shallow water bathymetry down to 5 m.

From the derived bathymetry three parameters were extracted: surface area covered by coral reefs, surface area not covered by coral reefs (down to 5 m depth) and the total shallow-water area. The surface area covered by coral reef is the area where satellite images manage to detect the corals at the water surface. The surface area not covered by coral reefs could still have corals and organisms at the seabed, but is referred to in this study as areas where coral reefs are not detected by the satellite images. In addition, the surface area not covered by corals was separated into 5 area sections (0-1m, 1-2m, 2-3m, 3-4m and 4-5m), in order to analyse sediment deposition in relation to flash floods.

4.3 The BQART model

Syvitski and Milliman (2007) developed the BQART model, which describes the relationship between geology, climate, water discharge and human impact. Within geology catchment area, lithology, topography and ice covers are the controlling factors. The model is used for predicting long-term (± 30 years) sediment load from rivers (eq. 4.1 and 4.2) (Syvitski and Milliman, 2007).

$$Q_s = \omega B Q^{0.31} A^{0.5} RT \quad \text{for T} \geq 2°\text{C}, \qquad \text{eq. 4.1}$$

$$Q_s = 2\omega B Q^{0.31} A^{0.5} R \quad \text{for T} < 2°\text{C}, \qquad \text{eq. 4.2}$$

Where Q_s is sediment flux (10^6 t/yr), ω is a constant of 0.0006 10^6 t/yr, B is a variable that takes geological and human factors into account, Q is water discharge (km^3/yr), A is area (km^2), R is the relief (km) and T is temperature (°C). The variable B is expressed as:

$$B = IL(1 - T_E)E_h, \qquad \text{eq. 4.3}$$

Where I is a glacial erosion factor ($I \geq 1$), L is a factor based on the average lithology within the catchment area, T_E is the trapping efficiency of lakes and man-made reservoirs, so that $(1 - T_E) \leq 1$, and E_h is a human-influenced soil erosion factor.

The lithology factor, L, is divided into six classes based on the hardness and erodibility of the rocks, where class one is the hardest and class six is the softest lithology, with the following values:

1) L = 0.5 is given to hard, acid plutonic and/or high-grade metamorphic rocks
2) L = 0.75 is given to mixed, but mostly hard lithology
3) L = 1.0 is given to volcanic rocks and carbonates, or a mixture of hard and soft lithologies
4) L = 1.5 is given to mixed, but mostly softer lithology
5) L = 2.0 is given to sedimentary rocks, unconsolidated sediments or alluvial deposits
6) L = 3.0 is given to the weakest material, including loess and crushed.

The anthropogenic factor, E_h, being the human impact on the landscape, is divided into three classes, based on what kind of impact humans have, and how severe the disturbance is on the landscape. Some of the ways humans affect the environment are urbanisation, deforestation and agriculture, and taking these factors into account Syvitski and Milliman (2007) defined E_h based on population density and per capita GNP:

1) $E_h = 0.3$ is given to catchments with high population density and a high GNP per capita.

2) $E_h = 1.0$ is given to areas with low human footprints

3) $E_h = 2.0$ is given where the population density is high but the per capita GNP is low.

Based on the 488 rivers in Syvitski and Milliman (2007) database, there exists a relationship between discharge, Q (in m^3/s), and drainage area, A (km^2), which is expressed in equation 4.4:

$$Q = 0.075A^{0.8} \qquad \text{eq. 4.4}$$

The BQART-model has been used in this study to estimate the yearly sediment load delivered from the catchments to the fan deltas and the coastal areas. In small, arid catchments dominated by infrequent high-discharge events, like the ones on the Sinai Peninsula, long-term sediment discharge is dependent on a few scattered events (Farnsworth and Milliman, 2003). Since rivers and catchments in the study area is dry for most of the year, mobilisation of sediments only really happen during flash flood event.

The catchment area and relief parameters are extracted from the DEM. Temperatures are derived from the dataset from Fick and Hijmans (2017) (see section 4.1.5). Water discharge is estimated from equation 4.4. All parameters used to estimate sediment flux are displayed in section 5.2.3.

5 RESULTS

The purpose of this chapter is to present the geomorphology of the southern Sinai Peninsula based on drainage analysis, mapped fan deltas and shallow-water areas down to 5 m depth. The nature, characteristics and distribution of these features will be described and relationships between catchments, deltas, coral reefs and shallow-water areas will be presented.

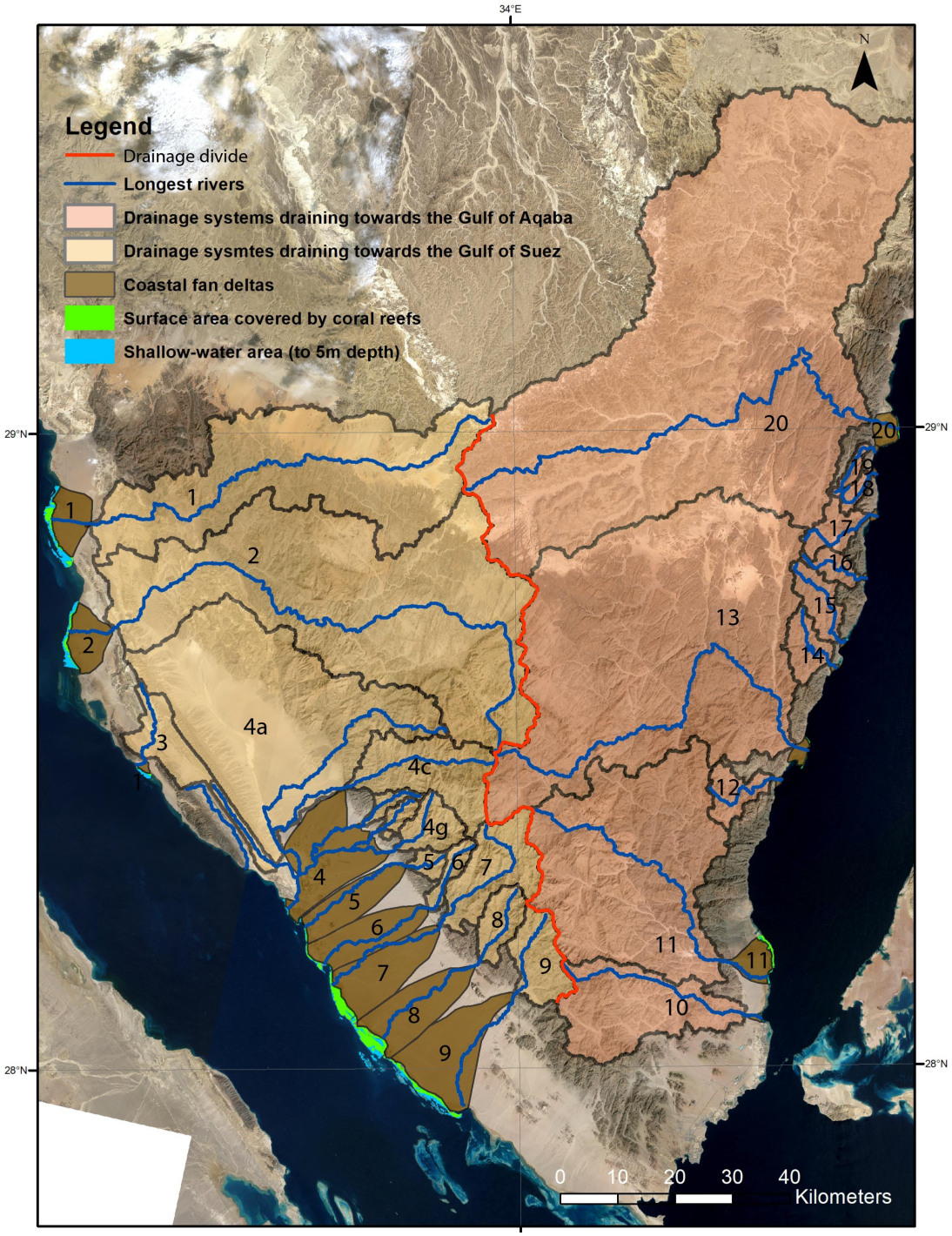

Figure 5.1 Image showing the drainage systems (catchment + fan) in the Sinai Peninsula, with shallow-water area and surface area covered by coral reef in front of the fans.

5.1 Drainage analysis

The data has been used to define the catchment areas and to determine its characteristics (Table 5.1).

Table 5.1 Main characteristics of the catchment areas of the Sinai Peninsula.

Catchment	Catchment area (sq.km)	Mean slope (deg)	Longest river (km)
Suez:			
1	1061,6	12,7	111
2	1761,0	15,3	140
3	119,7	9,7	21
4a	1127,1	13,0	77
4b	33,1	8,9	33
4c	250,4	26,4	74
4d	24,5	23,0	44
4e	23,9	26,4	39
4f	3,2	14,5	25
4g	81,1	26,0	45
5	26,8	21,5	34
6	38,5	24,5	41
7	197,5	25,4	60
8	77,6	25,5	45
9	125,0	23,4	47
Aqaba:			
10	358,5	18,0	45
11	1030,8	22,5	71
12	71,9	21,4	20
13	2067,0	16,9	97
14	68,8	20,1	19
15	75,2	20,0	24
16	39,6	19,0	17
17	62,4	19,0	19
18	21,4	24,3	13
19	21,1	22,2	13
20	3505,5	12,8	129

The drainage systems on Sinai Peninsula can be divided in two distinct areas, the western area that drains westward towards the Gulf of Suez and the eastern area draining towards the Gulf of Aqaba. Both areas includes three large catchments (1, 2 and 4a towards Suez and 11, 13 and 20 towards Aqaba) and several smaller catchments. The drainage systems investigated in this study drain from the high mountains in central Sinai, which are predominantly composed of igneous-metamorphic rocks. The large catchments all have areas exceeding 1000 km^2,

while the rest of the catchments are significantly smaller with the largest being 358 km^2. However, most of them are less than 100 km^2.

River Profiles

For each of the Sinai catchments the longest stream (river) was extracted and longitudinal profiles created along the stream paths. The profiles are displayed in Figure 5.2 and illustrate the lower gradients for the largest catchments (catchments 1, 2, 13, 20) and the steeper nature of the smaller catchments (Table 5.1; Figure 5,2).

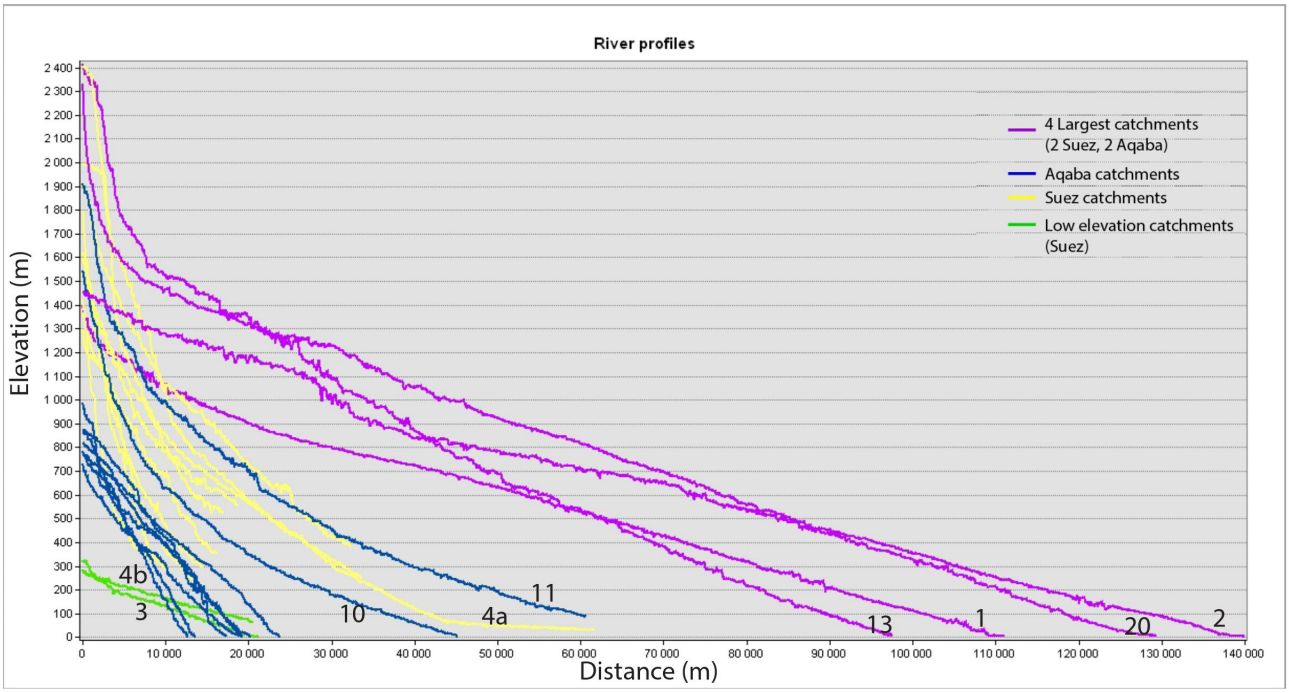

Figure 5.2 River profile extracted from the longest river from each catchment.

The profiles from the small catchment areas show a near-linear character of the river path, indicating an even and steep gradient throughout the catchments. This is the case for both the Aqaba and Suez catchments, even though the Suez catchments show a little concave up style. The four largest catchments, 1, 2 13 and 20, have much longer river paths with shallower gradient, but also having river profiles that are close to linear. Catchments 4a, 10 and 11 are exceptions to the near-linear trend and have a clear concave up shape (Figure 5.2). Catchments

reaching higher than 1500 m show a dramatic increase in gradient in the upstream area, illustrated on profile 2, 11 and 13, which show the steep nature of the highest areas on the Sinai Peninsula. Figure 5.2 indicates that there is a relationship where the largest catchment areas have longer rivers and shallower mean gradients. The exceptions seem to be catchments 3 and 4b, which have small areas, low gradients and lower relief (Figure 5.2).

5.2 Coastal environments

This section will look at the depositional end of the drainage systems along the coasts of Sinai, including the coastal fan deltas and the shallow-water areas associated with the fan deltas (Figure 5.1). The shallow-water areas are made up of coral reefs that build onto the delta front and areas where coral to not reach the surface. Two flash flood events have also been studied and are presented in section 5.3.

5.2.1 Coastal fan deltas

The coastal fan deltas mapped around the Sinai Peninsula are displayed in Figure 5.1 and the characteristics (area, gradient, shoreline and radius) of the fan deltas are presented in Table 5.2.

Table 5.2 Main characteristics of the fan deltas along the coast of the Sinai Peninsula

Fan	Fan area (sq.km)	Slope (deg)	Shoreline (km)	Radius (km)
Suez:				
Fan 1	59,0	4,8	14,50	7,0
Fan 2	60,9	4,6	13,60	8,4
Fan 3	2,7	5,1	3,10	1,9
Fan 4	205,9	6,5	6,50	20,2
Fan 5	99,6	5,3	5,00	20,9
Fan 6	116,0	5,8	8,50	21,5
Fan 7	139,0	6,2	10,60	21,2
Fan 8	140,9	6,4	11,00	21,6
Fan 9	188,8	7,7	18,10	23,3
Aqaba:				
Fan 10	2,3	4,5	1,70	3,1
Fan 11	36,9	3,0	10,70	7,1
Fan 12	1,5	3,8	2,40	1,4
Fan 13	10,3	3,5	8,70	3,2
Fan 14	1,3	3,3	2,10	1,3
Fan 15	1,1	4,2	2,20	1,0
Fan 16	0,8	3,0	1,60	1,0
Fan 17	2,0	3,9	3,00	1,4
Fan 18	1,0	3,4	2,10	1,0
Fan 19	0,9	5,1	1,30	1,2
Fan 20	21,3	3,1	8,80	5,4

Even though there are no obvious differences in area sizes of the catchments between those draining towards the Gulf of Suez and those draining to the Gulf of Aqaba (Table 5.1), there are distinct differences in the area sizes of the fan deltas. The data show that all of the deltas along the Gulf of Suez, except fan 3, are larger in size than the fans along the Gulf of Aqaba (Figure 5.3). Moreover, all Aqaba fans are less than 50 km^2, with the majority of them being less than 10 km^2 (Table 5.2). This indicates that the basin differences between the two gulfs, i.e. the steep basin margins and very deep Gulf of Aqaba vs. the shallower Gulf of Suez, are affecting geometry of the fans.

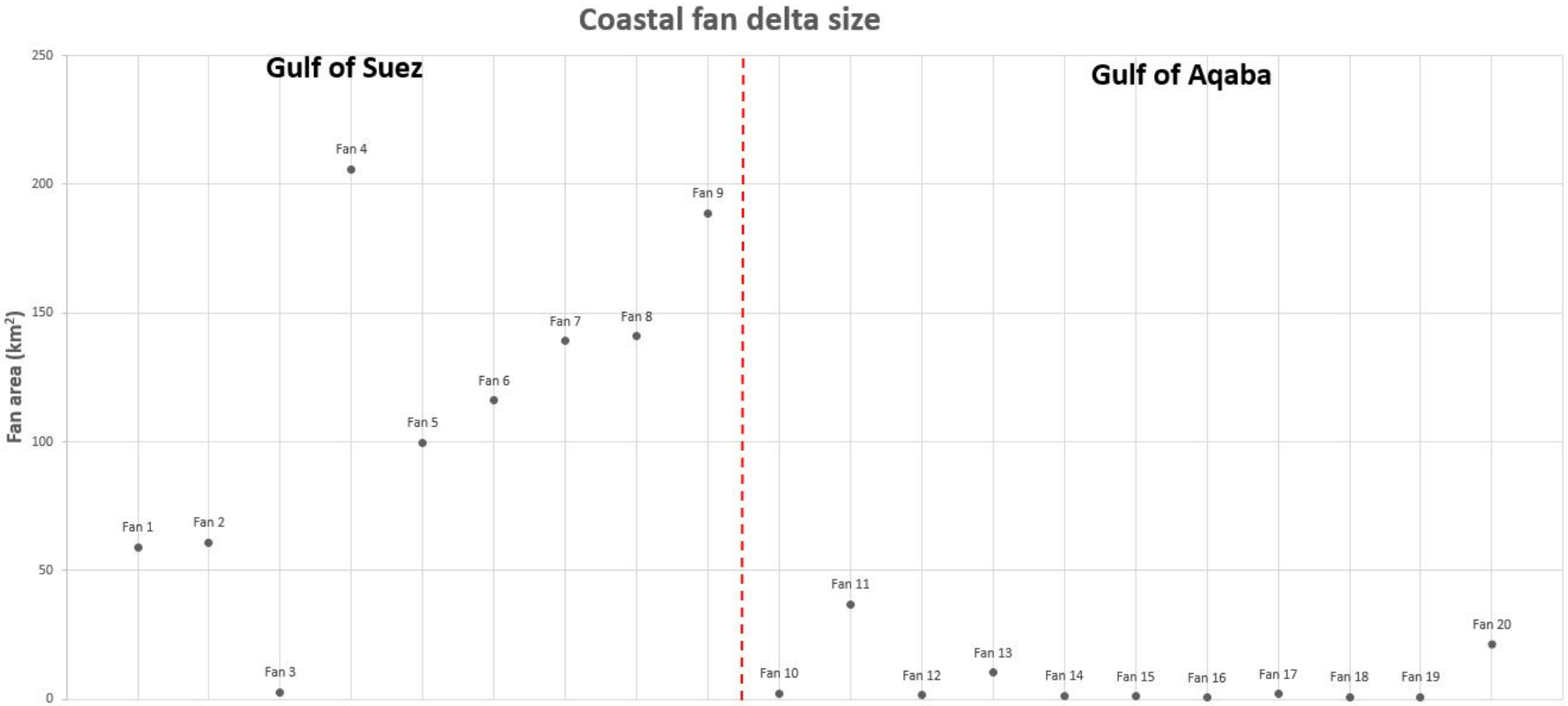

Figure 5.3 Area of all the mapped fans in Gulf of Suez and Gulf of Aqaba.
The coastal fan deltas are generally larger along the Gulf of Suez than along the Gulf of Aqaba.

Catchment area vs. fan area

Along the southern part of the Gulf of Suez the fan deltas show a more complex nature, as fans 4 through to 9 having coalesced into laterally amalgamating fans, covering a total area of 890 km^2 along the coast. These fans are larger than the rest of the mapped fan deltas, while their associated catchment areas are among the smallest ones (Table 5.3).

Table 5.3 A comparison of catchment area and fan area for each mapped drainage system.

Fan	Fan area (sq.km)	Catchment	Catchment area (sq.km)
Suez:		**Suez:**	
Fan 1	59,0	**1**	1061,6
Fan 2	60,9	**2**	1761,0
Fan 3	2,7	**3**	119,7
Fan 4	205,9	**4**	1543,34
Fan 5	99,6	**5**	26,8
Fan 6	116,0	**6**	38,5
Fan 7	139,0	**7**	197,5
Fan 8	140,9	**8**	77,6
Fan 9	188,8	**9**	125,0
Aqaba:		**Aqaba:**	
Fan 10	2,3	**10**	358,5
Fan 11	36,9	**11**	1030,8
Fan 12	1,5	**12**	71,9
Fan 13	10,3	**13**	2067,0
Fan 14	1,3	**14**	68,8
Fan 15	1,1	**15**	75,2
Fan 16	0,8	**16**	39,6
Fan 17	2,0	**17**	62,4
Fan 18	1,0	**18**	21,4
Fan 19	0,9	**19**	21,1
Fan 20	21,3	**20**	3505,5

The relationship between the catchment areas and delta size has been analysed and is represented in Table 5.3. Figures 5.4 and 5.5 display this relationship for the Gulf of Suez and Gulf of Aqaba, respectively. From these figures there is no clear relationship between the drainage area and the size of the delta. The Gulf of Suez (Figure 5.4) shows no correlation between the two parameters. However the Gulf of Aqaba (Figure 5.5) indicates that there is a relationship, where larger catchment areas are associated with larger fan deltas.

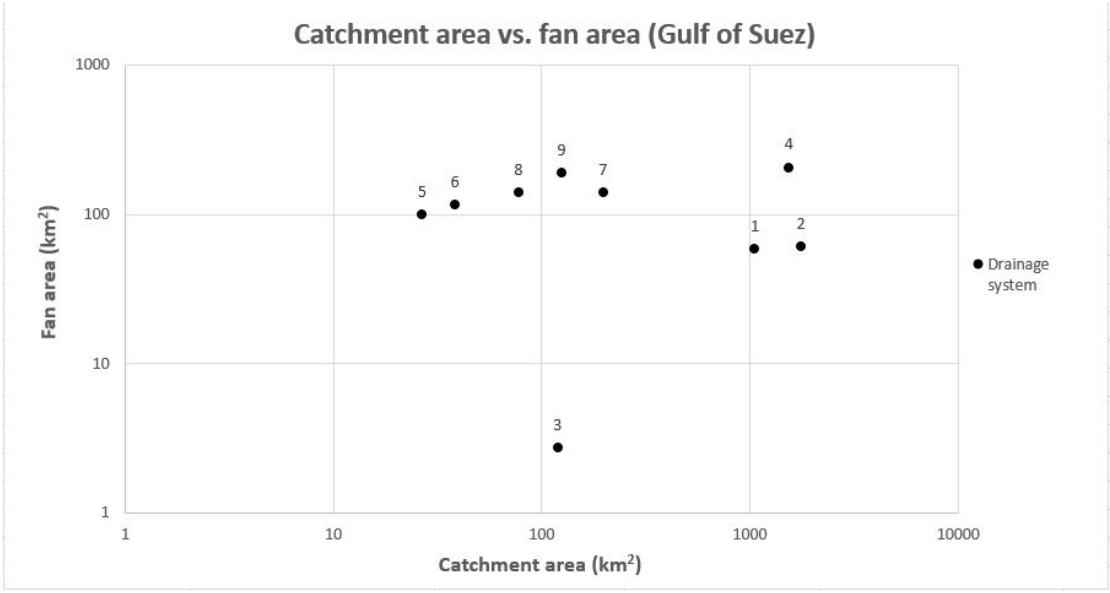

Figure 5.4 Fan area vs. catchment area for the studied drainage systems draining towards the Gulf of Suez.

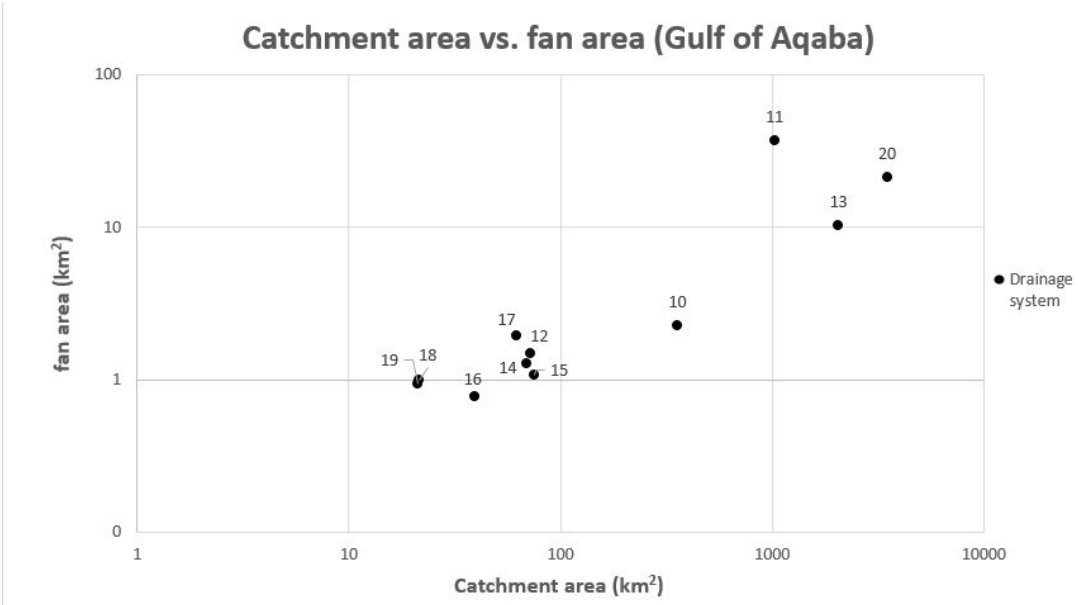

Figure 5.5 Fan area vs. catchment area for the studied drainage systems draining towards the Gulf of Aqaba. Note that y-axis changes from Figure 5.4.

Figure 5.6 depicts four of fan deltas from the study area (two from Suez and two from Aqaba) using satellite images from 1988 and 2019. These images illustrate that there has been little to no apparent or detectable progradation of the fans over the last 40 years that Landsat missions have been active. This suggests slow rates of progradation along the Sinai coasts. The active channels on the deltas, however, have changed over this period, most evident on fan 2 where the active distributary channels were running towards the southwest on the fan in 1988, while the fan today have active distributaries going towards the northwest (Figure 5.6a and 5.6b).

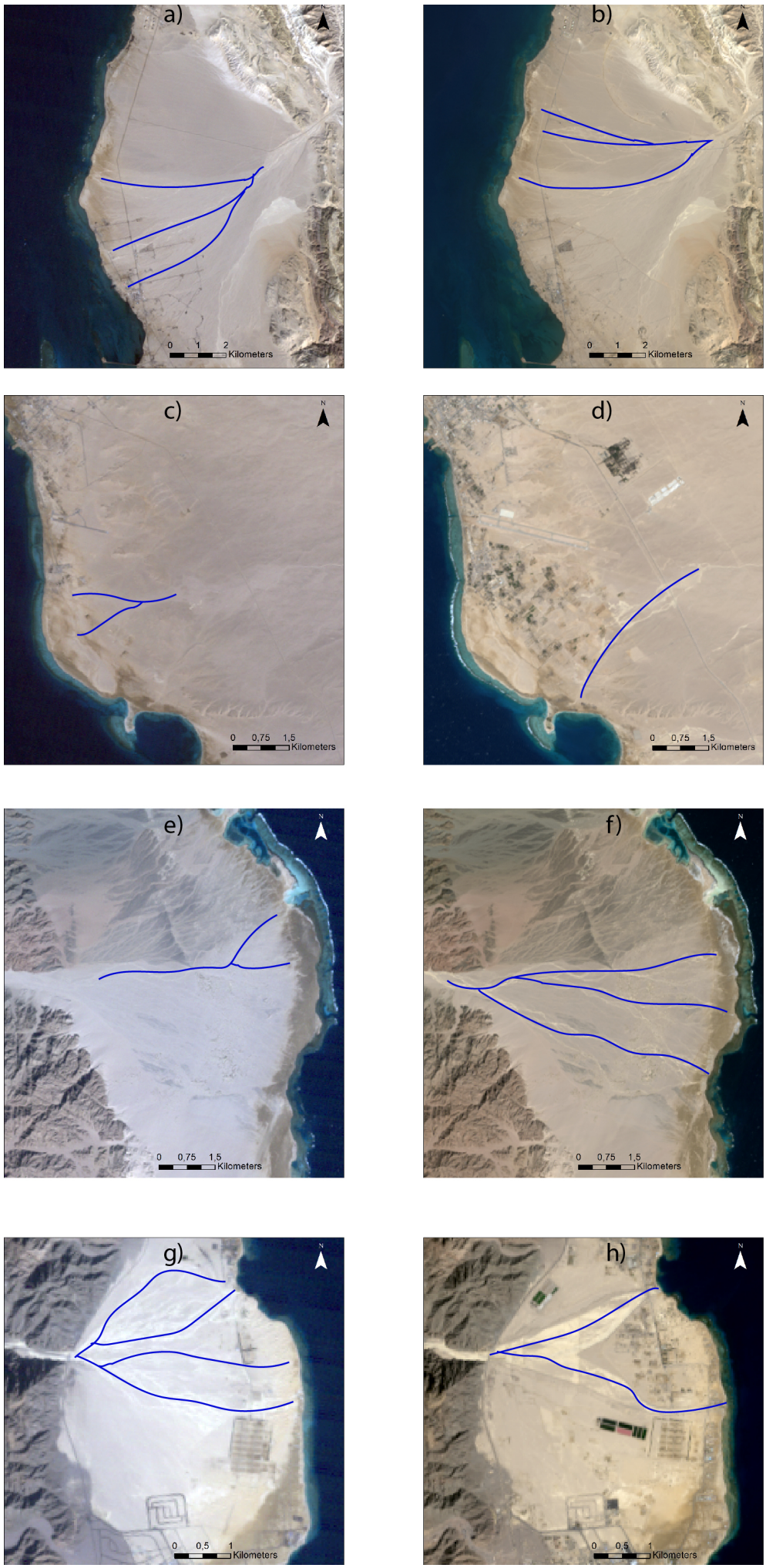

Figure 5.6 Landsat satellite images of 4 fans in the study area. Images on the left are from 1988 and images on the right are from 2019. a) and b) are Fan 2, c) and d) are fan 6, e) and f) are fan 11 and g) and h) are fan 20. Blue lines are interpreted active distributary channels.

5.2.2 Shallow-water environment

The shallow-water areas in this study are the surface areas from where the fan deltas reach the seawater and going out to where the water depth reaches 5 m. This area is split up into two distinct areas: 1) Area where coral reefs colonise on fan deltas and 2) Area corresponding to 0-5 m depth, where coral do not reach the water surface (Figure 5.1; Table 5.4).

Table 5.4 Estimated areas for the fans and for the marine areas in front of the fans. The shallow-water area in this table is the area where coral reefs do not reach the surface and therefore not detected on satellite derived bathymetry.

Fan	Fan area (sq.km)	Surface area covered by coral reefs (sq.km)	Shallow-water area (to 5m depth)	Total area (shallow-water + coral reef)	coral : total
Fan 1	59,0	5,69	9,3	14,99	0,38
Fan 2	60,9	3,48	6,5	9,98	0,35
Fan 3	2,7	0,43	0,8	1,23	0,35
Fan 4	205,9	0,41	1,5	1,91	0,21
Fan 5	99,6	0,80	0,9	1,70	0,47
Fan 6	116,0	1,71	1,1	2,81	0,61
Fan 7	139,0	10,31	1,6	11,91	0,87
Fan 8	140,9	11,00	6,8	17,80	0,62
Fan 9	188,8	6,90	8	14,90	0,46
Fan 10	2,3	0,08	0,1	0,18	0,45
Fan 11	36,9	3,14	0,7	3,84	0,82
Fan 12	1,5	0,01	0,05	0,06	0,11
Fan 13	10,3	0,77	0,4	1,17	0,66
Fan 14	1,3	0,04	0,03	0,07	0,58
Fan 15	1,1	0,11	0,1	0,21	0,53
Fan 16	0,8	0,04	0,06	0,10	0,38
Fan 17	2,0	0,01	0,1	0,11	0,10
Fan 18	1,0	0,00	0,03	0,03	0,00
Fan 19	0,9	0,01	0,08	0,09	0,06
Fan 20	21,3	0,68	0,3	0,98	0,70

Coral reefs

All the coral reefs analysed in this study are found on the fan deltas, corresponding to the delta-top type (Bosence, 2005). The surface areas occupied by coral reefs is different between the Gulf of Suez (~140 km^2) and the Gulf of Aqaba (~20 km^2). On average, larger surface areas are covered by coral reefs on the fan deltas in the Gulf of Suez (Table 5.4).

There are some detectable relationships between the surface area covered by coral reefs and the size and geometry of the fan deltas (Figures 5.7 and 5.8). The surface area covered by corals along a fan seems to increase with the area of the fan delta (Figure 5.7). Also, there seems to be a relationship between the area covered by coral reefs and the length of the delta shoreline: longer shorelines seem to be associated with larger surface areas covered by coral reefs (Figure 5.8). These results suggest that there is a trend within the study area where larger fan deltas are associated with larger surface areas covered by coral reefs.

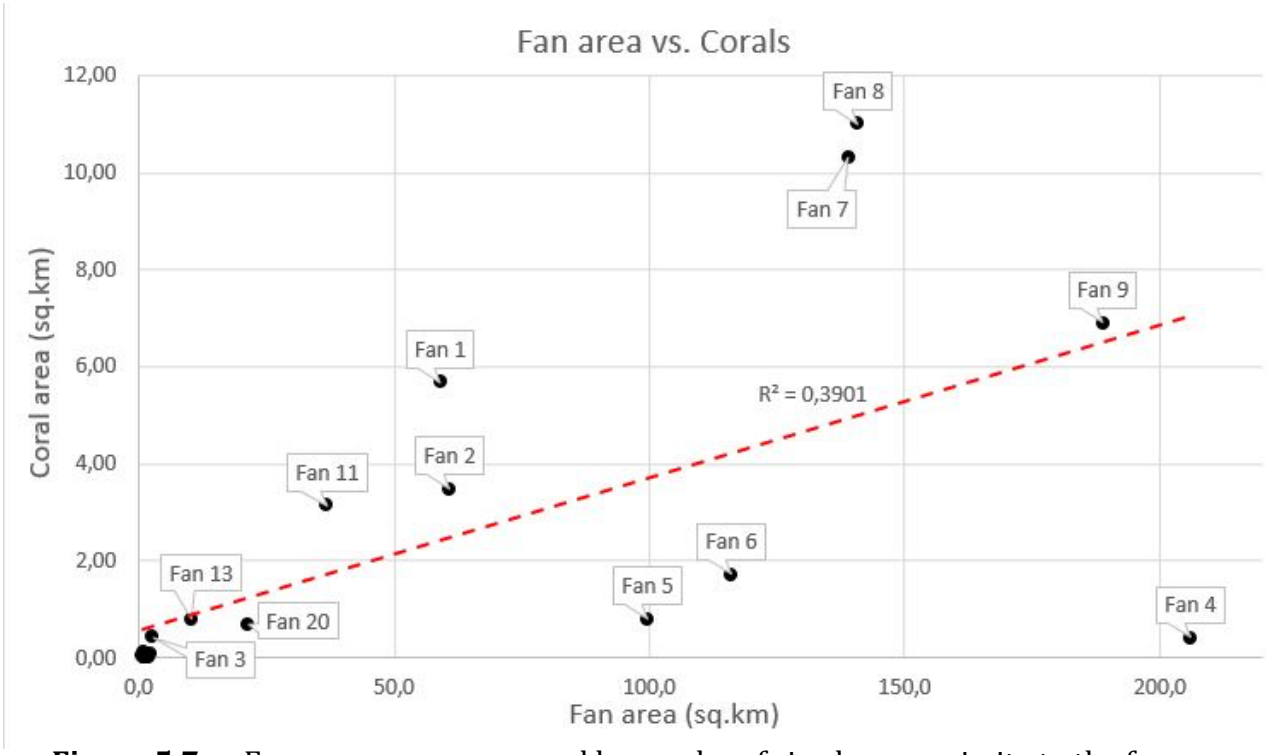

Figure 5.7 Fan area vs. area covered by coral reefs in close proximity to the fans.

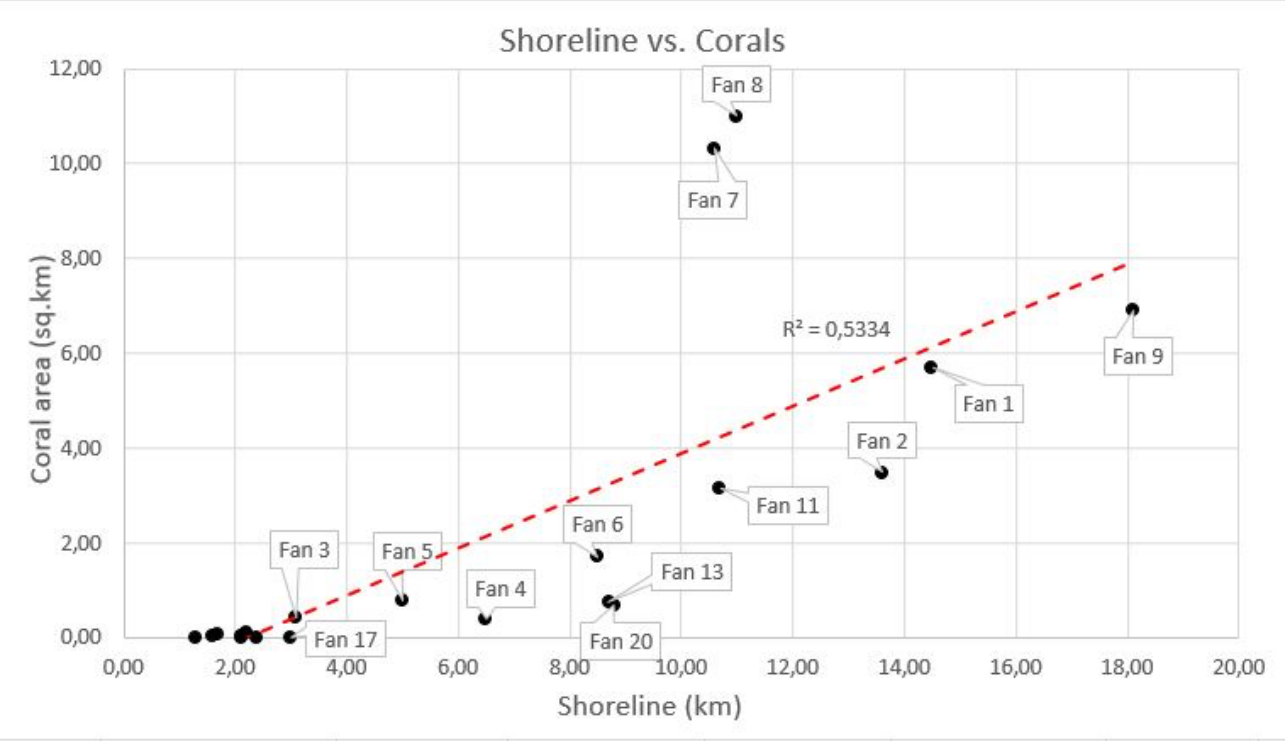

Figure 5.8 Length of shoreline for each of the studied fans vs. area covered by coral reefs for each fan.

Shallow-water bathymetry

The 0-5 m bathymetry is small and narrow throughout the study area. None of the studied fans have a shallow-water area more than 10 km^2 related to them, with most having ~1 km^2 or less of area reaching down to 5 m depth (Table 5.4). These narrow, shallow-water areas illustrate the rapid deepening of the basins, especially in the Gulf of Aqaba where depths between 200-1000 m are reached only 5-10 km off the coast. The Gulf of Suez does not have this same extreme depth gradient. However, there are areas that quickly reach depths of 40-60 m.

Coral area and 0-5 m depth area are added together to estimate the total shallow-water area in front of each coastal fan (Table 5.4). The ratios were calculated in order to illustrate how much of the total shallow-water area is occupied by corals. On average the corals make up 40-50 % of the area, but the proportion of corals varies from fan to fan. In the Gulf of Suez the ratio is varying from 21-87 %, while in the Gulf of Aqaba the ratio is varying from 0-82 % (Fan 18 had no detectable coral reefs at the water surface) (Table 5.4).

5.2.3 Sediment flux (Q_s) based on BQART model

The sediment flux from each catchment was calculated using the BQART model (chapter 4.4). Catchment area and relief are extracted from the DEM, discharge (Q) is calculated from equation 4.4, temperature calculation is explained in chapter 4.3 and factor B (eq 4.3) is given the value 1.5 as the lithology of the Sinai Peninsula is hard, crystalline basement with no glacial influence (I=1) and low human activity (E_h=1 and 1-T_E=1), making B = L = 1.5. The parameters and resulting calculations are presented in Table 5.5. The resulting calculations show that the largest catchments are associated with the highest yearly sediment load. It is the catchment area and relief parameters that varies the most between the catchments, while the rest of the parameters have little or no variation, indicating that it is the size of the catchments that largely controls the sediment flux in Sinai (Table 5.5).

Table 5.5 Parameter in the BQART model and the calculated yearly sediment load.

Catchment	Catchment area (sq.km)	Relief (km)	B	w	Discharge, Q (km^3/yr)	Annual mean temp (deg C)	Sediment load, Q_s (10^6 t/year)
1	1061,6	1,6	1,5	0,0006	0,62	19,9	0,82
2	1761,0	2,6	1,5	0,0006	0,93	19,1	1,86
3	119,7	0,7	1,5	0,0006	0,11	22,3	0,07
4a	1127,1	2,2	1,5	0,0006	0,65	22,0	1,28
4b	33,1	0,4	1,5	0,0006	0,04	23,0	0,02
4c	250,4	2,6	1,5	0,0006	0,20	17,6	0,39
4d	24,5	1,9	1,5	0,0006	0,03	20,5	0,06
4e	23,9	1,8	1,5	0,0006	0,03	19,6	0,05
4f	3,2	0,7	1,5	0,0006	0,01	22,8	0,01
4g	81,1	2,3	1,5	0,0006	0,08	18,9	0,16
5	26,8	1,7	1,5	0,0006	0,03	20,8	0,06
6	38,5	2,5	1,5	0,0006	0,04	19,1	0,10
7	197,5	2,5	1,5	0,0006	0,16	17,7	0,32
8	77,6	2,4	1,5	0,0006	0,08	18,7	0,16
9	125,0	2,3	1,5	0,0006	0,11	18,7	0,22
10	358,5	2,0	1,5	0,0006	0,26	21,7	0,50
11	1030,8	2,4	1,5	0,0006	0,61	20,3	1,21
12	71,9	1,2	1,5	0,0006	0,07	21,7	0,09
13	2067,0	2,5	1,5	0,0006	1,06	19,1	2,01
14	68,8	0,9	1,5	0,0006	0,07	21,9	0,07
15	75,2	1,0	1,5	0,0006	0,07	21,4	0,07
16	39,6	0,9	1,5	0,0006	0,04	21,4	0,04
17	62,4	1,0	1,5	0,0006	0,06	20,6	0,06
18	21,4	1,0	1,5	0,0006	0,03	20,4	0,03
19	21,1	1,0	1,5	0,0006	0,03	20,6	0,03
20	3505,5	1,6	1,5	0,0006	1,62	18,6	1,89

5.3 Flash floods

Flash floods are the main process transporting sediments from the catchment areas to the coastal fan deltas and into the two gulfs. In this thesis two flash flood events have been studied where the focus has been on the shallow-water bathymetry (0-5 m depth). Three satellite derived bathymetric models were generated for each flash flood event: 1) a bathymetric model obtained from the most recently acquired imagery before the flash flood (within 1 month); 2) a bathymetric model obtained from the first possible acquired imagery after the flash flood (within 2 months); 3) a bathymetric model obtained from satellite imagery acquired approximately one year after the flash flood. This was done to investigate if there are any detectable differences before and after the flooding event, which would be a sign of deposition. Moreover, the third bathymetry was derived to examine if marine processes, such as long shore drift, remove the potentially deposited sediments. The two flash flood events investigated in this study are the November-December of 2002 and the October-November of 2016. The flash flood of 2002 was described by Hermas et al. (2010) as a high magnitude flash flood, with 40 mm of precipitation. The 2016 flash flood was documented by FloodList (2016), caused by four days of extreme rainfall, with peak precipitation of 51 mm in 24 hours. Both of these events by far exceeded the average yearly precipitation, in only a few days.

2002 flash flood event

To investigate the flash flood of 2002, two sets of Landsat 7 images and one set of Landsat 5 images were used. The first set was collected at 7th (Suez) and 16th (Aqaba) of September 2002 and the second set was collected at 28th of December 2002 (Suez) and 6th of January 2003 (Aqaba). Both of these sets are Landsat 7 images. The last set, which is Landsat 5, was collected at 11th (Aqaba) and 18th (Suez) of September 2003. Landsat 5 images were used for the last set because Landsat 7 has an error on all images acquired from mid-2003 to 2010.

Table 5.6 Table showing area of the estimated shallow-water bathymetry (0-5 m depth) in front of the studied fans, for the flash flood event in 2002. It shows the area where corals do not reach the surface, as it is this area that SDB manage to estimate depth values. (All numbers are in square km)

Fan name	Pre-flood (sept 2002)	Post-flood (des 2002)	Deposition	One year late (sept 2003)	Sediment removal
1	9,38	15,80	6,41	8,42	-7,38
2	6,65	7,22	0,57	6,59	-0,63
3	1,68	1,42	-0,26	1,90	0,48
4	1,38	1,07	-0,31	1,49	0,42
5	1,43	1,14	-0,29	1,72	0,58
6	2,34	1,74	-0,60	3,15	1,41
7	3,99	3,02	-0,97	4,86	1,84
8	6,63	3,69	-2,93	5,73	2,03
9	9,63	7,58	-2,05	9,90	2,32
10	0,16	0,16	0,00	0,18	0,02
11	0,99	0,82	-0,17	1,08	0,26
12	0,07	0,07	0,01	0,09	0,01
13	0,46	0,51	0,05	0,56	0,05
14	0,03	0,06	0,02	0,05	0,00
15	0,17	0,15	-0,02	0,20	0,05
16	0,08	0,09	0,01	0,10	0,00
17	0,12	0,16	0,04	0,16	0,00
18	0,05	0,07	0,02	0,06	0,00
19	0,09	0,11	0,02	0,09	-0,01
20	0,51	0,57	0,06	0,58	0,01

For most of the shallow-water areas there is little to no detectable changes from before to after the flash flood (Table 5.6). The exception, however, is fan 1, which shows a clear increase in shallow-water area reaching 5 m depth. This indicates that there was sediment deposition in front of this fan that was detectable on satellite derived bathymetry. Moreover, the area in front of fan 1 decreased by a significant amount one year after, which points to sediment removal from this area.

A more detailed analysis was done on the shallow-water area in front of fan 1 (Table 5.7). The shallow-water area was split into 5 sections, a section for each metre of depth (0-1m, 1-2m, etc.). This analysis shows that the biggest changes happened in the 4-5 m depth range (Table 5.7).

Table 5.7 Detailed analysis in front of fan 1 before and after the flash flood of 2002. It shows the area where corals do not reach the surface, as it is this area that SDB manage to predict depth values. (All numbers are in square km)

	Pre-flood (sept 2002)	Post-flood (des 2002)	Deposition	One year later (sept 2003)	Sediment removal
Fan 1 depths:					
0-1m	1,42	1,12	-0,30	1,39	0,27
1-2m	1,26	1,59	0,34	1,28	-0,31
2-3m	1,49	1,99	0,51	1,57	-0,42
3-4m	2,28	3,80	1,52	1,97	-1,83
4-5m	2,94	7,30	4,35	2,21	-5,08

2016 flash flood event

Three sets of Landsat 8 satellite images were used to investigate the 2016 flash flood. The first set of images was acquired at 21st (Suez) and 30th (Aqaba) of September 2016. The second set was acquired after the flooding event at 4th (Aqaba) and 11th (Suez) of January 2017, which was the satellite image set after the flood that the whole study area was cloud-free. The last set was acquired at 8th (Suez) and 17th (Aqaba) of September 2017.

Table 5.8 Table showing the area of the shallow-water area(0-5 m depth) in front of the studied fans, for the flash flood event of 2016. It shows the area where corals do not reach the surface, as it is this area that SDB manage to estimate depth values. (All numbers are in square km)

Fan name	Pre-flood (oct 2016)	Post-flood (jan 2017)	Deposition	One year later (oct 2017)	Sediment removal
1	9,3	14,3	5	10,00	-4,30
2	6,5	10,8	4,3	11,30	0,50
3	0,8	0,7	-0,1	1,00	0,30
4	1,5	1,7	0,2	1,80	0,10
5	0,9	0,9	0	0,80	-0,10
6	1,1	0,9	-0,2	1,70	0,80
7	1,6	1,7	0,1	3,10	1,40
8	6,8	6	-0,8	6,60	0,60
9	8	6,6	-1,4	8,20	1,60
10	0,1	0,4	0,3	0,20	-0,20
11	0,7	1,3	0,6	1,00	-0,30
12	0,05	0,08	0,03	0,04	-0,04
13	0,4	0,7	0,3	0,50	-0,20
14	0,03	0,4	0,37	0,03	-0,37
15	0,1	0,1	0	1,00	0,90
16	0,06	0,09	0,03	0,08	-0,01
17	0,1	0,2	0,1	0,08	-0,12
18	0,03	0,07	0,04	0,02	-0,05
19	0,08	0,2	0,12	0,08	-0,12
20	0,3	0,5	0,2	0,48	-0,02

In the analysis for this flash flood, fans 1 and 2, show a clear increase in shallow-water area reaching 5 m depth. This indicates that there was sediment deposition in front of these two fans that were detectable on satellite derived bathymetry (Figure 5.9). Moreover, the area in front of fan 1 decreased by a ~4 km^2 one year after the flood (Table 5.8), which points to sediment removal from this area.

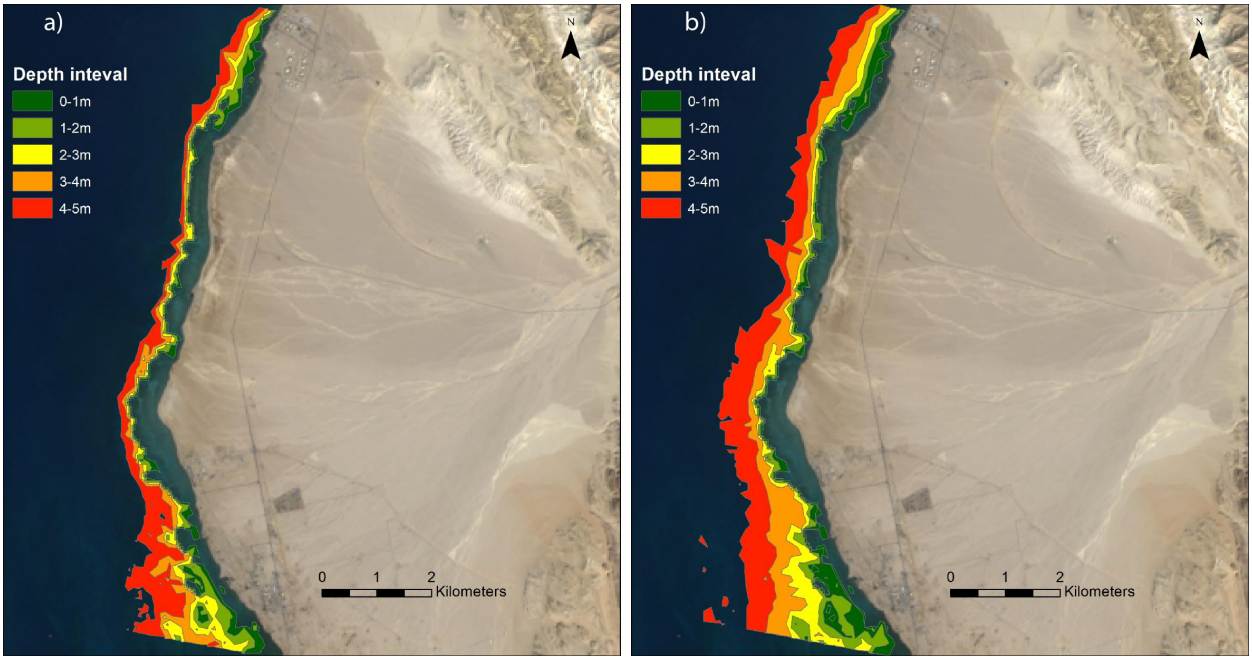

Figure 5.9 The shallow-water area down to 5 m depth in front of fan 2 (area without coral reefs at the surface) a) before and b) after the flash flood of October-November 2016. Satellite derived bathymetry detected an increase of this area, and the 4-5m interval expanded the most.

A more detailed analysis was done in front of the two fans that showed a clear increase in shallow-water area (Table 5.9). The shallow-water area was split into 5 sections, a section for each metre of depth (0-1m, 1-2m, etc.) with both fan 1 and 2 showing a big increase in the interval of 4-5 m depth. It is also these areas that shows the largest loss of sediments, indicating that the sediments deposited after the flood are being removed.

Table 5.9 Detailed analysis in front of fan 1 and 2 before and after the flash flood of 2016. It shows the area where corals do not reach the surface, as it is this area that SDB manage to predict depth values. (All numbers are in square km)

	Pre-flood (oct 2016)	Post-flood (jan 2017)	Deposition	One year later (oct 2017)	Sediment removal
Fan 1 depths:					
0-1m	0,88	1,19	0,30	1,33	0,14
1-2m	1,14	1,58	0,45	1,54	-0,05
2-3m	1,65	2,27	0,63	1,85	-0,42
3-4m	2,06	2,89	0,82	2,51	-0,38
4-5m	3,51	6,31	2,80	2,80	-3,51
Fan 2 depths:					
0-1m	0,96	1,27	0,31	2,24	0,97
1-2m	0,99	1,25	0,27	1,37	0,12
2-3m	0,99	1,51	0,52	1,91	0,40
3-4m	1,22	2,63	1,41	2,88	0,25
4-5m	2,37	4,17	1,80	2,90	-1,27

The analysis of the 2002 and 2016 flash flood events show that the biggest changes are happening in the northern parts of the study area, in the Gulf of Suez (Fan 1 and Fan 2). This points to an area where deposition of sediments are more easily detectable on satellite derived bathymetry, whereas conditions in front of the other fans might make it difficult for sediments to accumulate in these areas. This is further discussed in section 6.1.

6 DISCUSSION

In this chapter key observations from the remotely sensed data will be discussed. The purpose is to address potential controls on spatial distribution and geometry of geomorphological features and depositional environments. Relationships between geomorphology and deposition will also be discussed to better understand how basin configuration affects the silicicalstic deposition and coral growth. Lastly, this chapter will discuss the validity of satellite derived bathymetry and its limitations in such a study.

6.1 Drainage on Sinai Peninsula

The southern part Sinai Peninsula is drained by 27 drainage systems (mapped in this study), draining into the mid to southern Gulf of Suez and mid to southern Gulf of Aqaba. Sediment supply from the catchments draining into the two gulfs is highly episodic as the hyper arid climate keeps the drainage pattern dry for most of the year, if not for the whole year (Roberts, 1987). The rain season tend to be limited to only a few day or weeks during the winter months, resulting in average yearly precipitation of only 10-25 mm. Heavy storm and rainfall events, which are rare and infrequent in the area, are needed in order to mobilise sediments from the catchment areas to the coast.

The total drainage catchment area mapped in this study of the Sinai Peninsula represents ~12 300 km^2. Most of this area is drained by only the six largest catchments, meaning that 86% of the total catchment area is drained by only 23% of the catchment area. Rowlands et al. (2014) found similar results for the Saudi-Arabian Red Sea, where only 10% of the catchment area drain 80% of the total drainage basin area of their study. None of the catchments that drain from the central, high-lying areas of southern Sinai have mean gradients lower than 10°, with mean gradients reaching as high as 26° for some of the smaller catchments (Table 5.1). Sediments found on alluvial fans and coastal fan deltas throughout the Red Sea, Gulf of Suez and Gulf of Aqaba tend to be of the coarser grain sizes, mostly medium to coarse sand and conglomerate (Purser et al., 1987; Bosence, 2005; Rowlands and Purkis, 2015). This can be explained by the steep

gradients found throughout the catchments draining the Sinai Peninsula (Table 5.1). The steep gradients and lack of unvegetated soils (due to hyper-arid conditions) maximise the effects of flash floods, carrying a coarse sediment load to the fan deltas (Roberts, 1987).

The drainage pattern on the southern Sinai Peninsula is dominated by transverse drainage systems, with all mapped fan deltas being sourced from transverse catchments (Figure 6.1). Transverse drainage is a common feature in other rift basins and the extensional settings. Examples from the Red Sea, the Basin and Range (USA) and central Greece all show transverse catchments dominating the drainage systems (Leeder and Jackson, 1993; Gawthorpe and Leeder, 2000; Rowlands et al., 2014). The exceptions in this study are catchments 4a and 4b, where catchment 4a has an axial and a transverse component and 4b is axially drained (Figure 6.1). The axial drainage is controlled by a basin-bounding fault

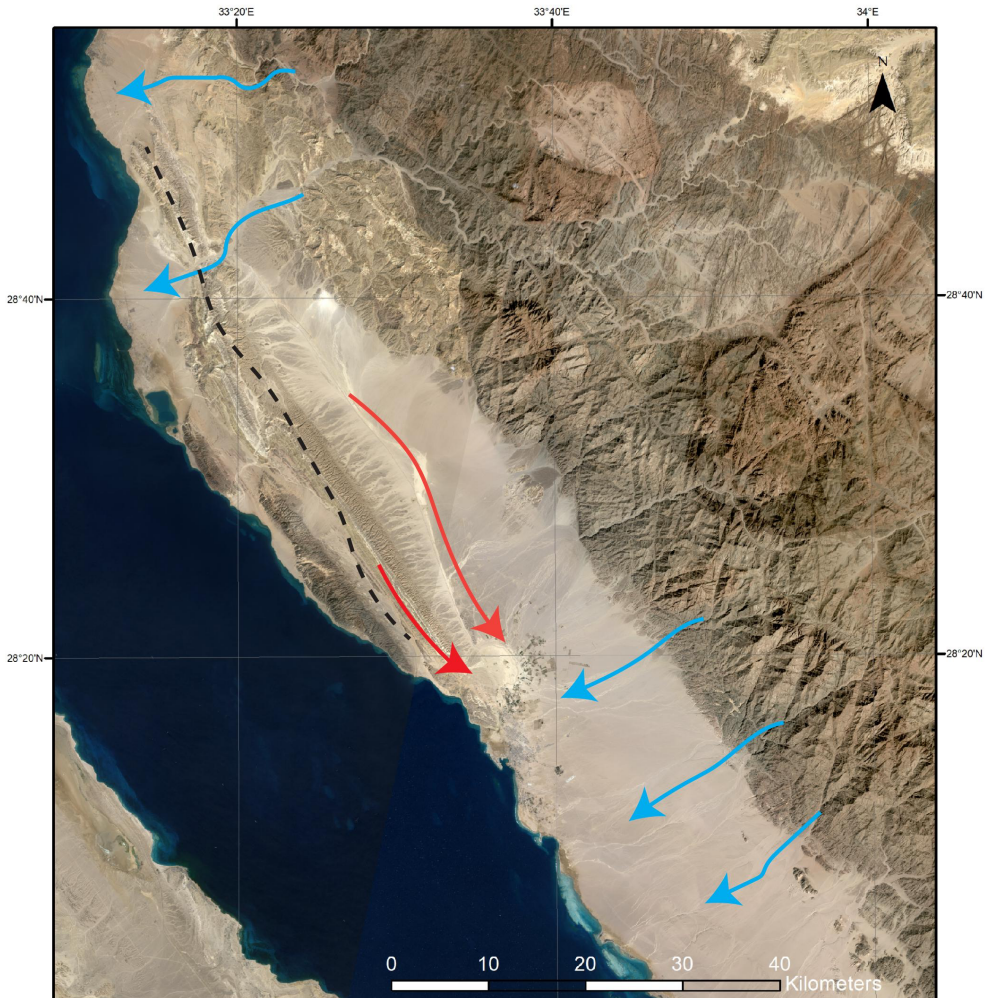

Figure 6.1 Transverse drainage (blue arrows) and axial drainage (red arrows) draining towards the Gulf of Suez. Black, dashed line illustrates the topographic high as a result of a rotated fault block, redirecting and causing the axial drainage.

located on the northwestern part of the study area (Gawthorpe and Colella, 1990; Sharp et al., 2000). This has created a topographic high onshore which dictates some of the drainage pattern in drainage system 4 (Figure 6.1).

The sediment flux calculations from the BQART-model suggest that larger catchments with higher relief supply more sediment to the coastal areas. The five catchments showing the highest sediment flux, catchments 2, 4a, 11, 13 and 20, have estimated fluxes of between 1-2x10^6 tons/year. This is 1 to 2 orders of magnitude larger then the estimated sediment flux from the smallest catchments (e.g. catchments 3, 4f and 18; Table 5.5). These estimations suggest that the majority of sediments drained from the Sinai Peninsula are derived from a few large catchments. Even though there are big differences within the Sinai Peninsula, on a global scale the estimated figures are quite small. This is mostly because the catchments in the study area are small on a global scale (Syvitski and Milliman, 2007). However, sediment delivery to the Sinai coastal areas is only limited to a short time interval (days or weeks), predominantly in the form of flash floods. Farnsworth and Milliman (2003) found for the arid Californian river, the Salinas River, the 70-year-average sediment load was only approached or exceeded 18 times during that 70-year period. Moreover, the total high-discharge time was less than 5 weeks of that 70-year period (Farnsworth and Milliman, 2003). Warrick and Milliman (2003) found similar results for the arid Santa Clara River in California, where 75% of its sediment load was transported in flash flood events in only 30 days over a 50-year period. Findings from these studies suggest that yearly sediment load calculations from the BQART-model in this study are not accurate. For most years, the BQART model will overestimate the sediment load, while underestimating the sediment load for years with severe flash flood events (Farnsworth and Milliman, 2003). As major flash flood events only happen once every few years, sediment delivery to the coastal area is highly variable from one year to the next (Issar and Gilad, 1982).

The analysis of two flash flood events in this study reveals that the shallow-water area (< 5m) in front of fans 1 and 2 increase in size after each event, with the increase in surface area varying from 4 to 6 km^2. The sediments transported

by flash floods accumulate in front of the fan deltas and contributing to their growth. Deposited sediments results in a decrease in water depth and thus, an increase of the shallow-water area. There could be several reasons why there are no clear variations observed in front of the other mapped fan deltas: 1) As catchments 1 and 2 are among the largest ones, more sediment is mobilised, which could make it easier to detect the variations; 2) Local variations in precipitation could give more rainfall to drainage system 1 and 2; 3) Landsat 8 satellite imagery has too low resolution to capture the variations in smaller areas. Satellite images with higher resolution could improve the results (see section 6.5).

6.2 Coral reefs located on the coastal fan deltas

The coral reefs mapped in this study are of the fringing reef type, separated from the coastline by only a narrow shallow-water section (Dullo and Montaggioni, 1998). These coral reefs are of the delta-top type described by Bosence (2005), where the coral reefs grow on top of the deltas building out into the shallow-water areas. More surface area covered by coral reefs is associated with the fan deltas in the Gulf of Suez than in the Gulf of Aqaba (Table 5.4). This seems to be associated with larger fans and larger shallow-water areas extending further into the Gulf of Suez basin. This study identifies that larger surface areas covered by coral reefs are associated with larger fan deltas with longer shorelines. Such an observation was also made by Rowlands et al. (2014), who identified that areas with longer coastlines in the Red Sea have larger areas occupied by coral reefs.

6.2.1 Flash flood impact on coral reefs

The detailed analysis of the flash flood on fans 1 and 2 showed that the interval of 4-5 m depth increased the most during both flash floods, whereas the shallower areas, as well as the area covered by corals, was almost unaffected. This suggests that most of the sediment flushed out by the flash flood were deposited ~500-1000 m from the coastline, rather then directly at the coastline. The fringing reefs associated with the fan deltas seem to cover the entire length of the fan shoreline, only interrupted where distributary channels feed into the basin (Dullo and Montaggioni, 1998). This is best shown on fan 2, where there is a small section in the centre of the fan with reduced area covered by coral reefs compared to the rest of the fan, which is located in front of an active distributary channel (Figure 6.2). Distributary channels on fan deltas in the Gulf of Suez and Gulf of Aqaba are well-defined and can continue as subaqueous channels where the channel reach the sea (Hayward, 1982; Roberts, 1987). Such channels usually transport most of the flash flood sediments past the coral reefs, keeping the organisms protected from being inundated by too much siliciclastic material (Roberts, 1987; Dullo and Montaggioni, 1998). Studies from the Gulf of Suez and Gulf of Aqaba suggest that well-defined channels combined with steep morphology can transport much of the sediments past the coral reef (Roberts, 1987; Dullo and Montaggioni, 1998). This could help explain why the biggest changes were observed in the deepest parts in front of fan 1 and 2 (4-5 m interval), as much of the sediments seem to be transported past very shallow areas. In addition, it is in this same depth interval that shows the biggest changes one year after both flash floods (Table 5.7; Table 5.9). This points to sediment removal during the year after the flooding events and can demonstrate the marine currents, at least in the Gulf of Suez. Strong winds from the North towards the South are known to occur throughout the year in both the Gulf of Suez and the Gulf of Aqaba (Roberts, 1987; Nir, 1996). These winds cause marine currents, mainly longshore drift, and wave action along the Sinai coasts, which, along with tidal currents, effectively removes sediments and suspended material from and around coral reefs after flash flood events (Hayward, 1982; Nir, 1996).

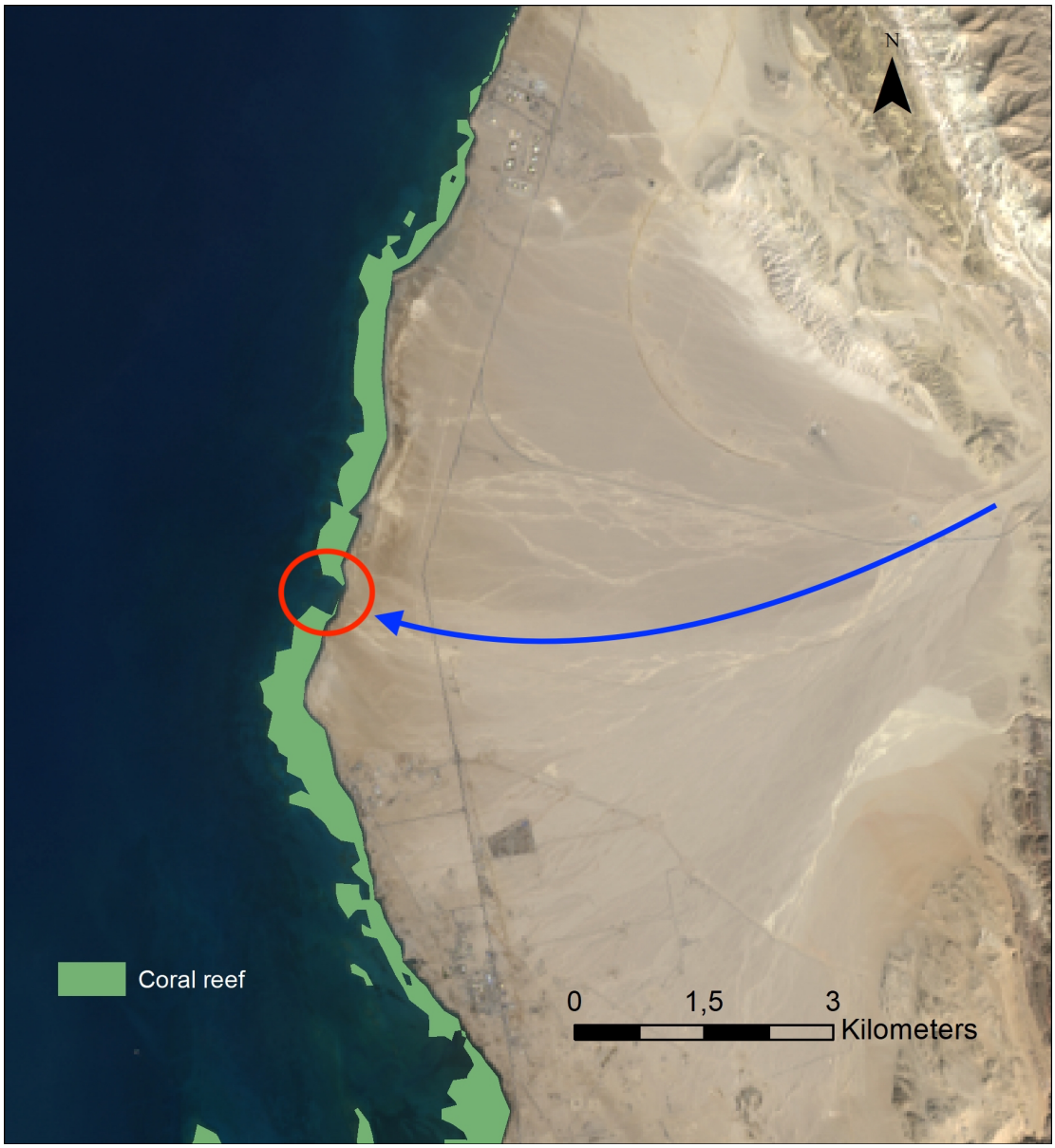

Figure 6.2 Gap (red circle) in the fringing coral reef reaching the water surface around Fan 2, in front of an active distributary channel (blue arrow). Indicating where the fan is most active and crating a pathway past the corals, minimising damage during flash floods.

6.3 Basin controls on coastal fan deltas

This study identifies that the coastal fan deltas in the Gulf of Suez are generally larger than the fan deltas in the Gulf of Aqaba (Table 5.2; Figure 5.3). This is the case, even though the catchments draining towards both gulfs are of roughly similar sizes (Table 5.1). The larger fan deltas in the Gulf of Suez could be explained by the different tectonic settings between the two gulfs. As the Gulf of

Suez is a rift basin, rotated and tilted fault blocks are found throughout the gulf. The subsiding hanging-walls creates accommodation space for coastal fan deltas to develop (Gawthorpe and Leeder, 2000). Since the Gulf of Aqaba is a pull-apart basin developed from a strike-slip fault, rotated fault blocks are absent in the gulf (Ben‐Avraham, 1985). Instead there is an abrupt drop in depth, creating steep slopes from the coastal area to the basin floor of the Gulf of Aqaba. The coastal area is therefore unable to trap sediments, with much of the sediments transported directly to the basin floor.

These observations suggest that the structural style of a basin is the primary control on the deposition of coastal fan deltas, and thus also on coral reef distribution. Bosence (2005) identifies that the tectonics are important for coral growth in rift basins like the Red Sea. The tectonics controls the basin topography; especially uplifted fault blocks can create shallow-water areas for corals to occupy. Rowlands et al. (2014) also emphasises the importance of bathymetric highs created by fault blocks in the Red Sea for coral reef development. The fault blocks are in addition important for creating depocentres in the coastal area where fan deltas can develop. This mechanism controls the development and geometry of coastal fan deltas in the Gulf of Suez (Gawthorpe and Colella, 1990). The Gulf of Aqaba is lacking these fault blocks, resulting in a narrow coastal area with little space for the coastal fans to expand or for coral reefs to colonise.

6.4 Climate controls on sediment delivery and coral reefs

While tectonics controls the basin configuration, drainage pattern, distribution of deposition and the long-term (10^5s-10^6s of years) stratigraphy, the climate is the primary control on the environmental conditions on a shorter (10^3s-10^4s of years) term (Roberts, 1987).

The Sinai Peninsula have an annual average temperature of around 20 °C and an average precipitation rate of 10-25 mm per year. Most of the rain precipitates in the high central part of Sinai, while the rainfall decreases towards the coastal

area and usually receive less than 10 mm a year (Hermas et al., 2010). The arid climate controls the delivery of sediment feeding the coastal fan deltas and into the gulfs. As flash floods are rare and infrequent, there is little suspended material in the seawater, creating clear-water conditions throughout the Gulf of Suez and Gulf of Aqaba (Purser et al., 1987). The high average temperatures keep the surface water temperature high throughout the year. The warm, arid and clear-water conditions of the Sinai Peninsula are ideal for coral growth in the shallow-water areas (Purser et al., 1987; Rowlands et al., 2014).

The arid climate controls sediment transport to the coastal areas, restricting progradation and further development of the coastal fan deltas. Low sediment transport, together with warm, clear water, favours the development of corals, as there are little suspended sediments in the two gulfs. Additionally, there is no stress from clastic input on the developed corals, making it possible for the reefs to occupy the available shallow-water space (Purser et al., 1987; Dullo and Montaggioni, 1998; Rowlands et al., 2014).

6.5 Limitations on Satellite derived bathymetry

Satellite derived bathymetry from Landsat satellite images was used to extract the shallow-water bathymetry, from which coral distribution and water depth down to 5 m was extracted. The method relies on precise and accurate depth soundings. The precision of the digitised depth soundings from the nautical charts is one of the uncertainties in this study, as there are uncertainties during georeferencing of the nautical charts in ArcGIS, as well as uncertainties when manually collecting depth soundings from the charts. The nautical chart for the Gulf of Aqaba has large areas without detailed surveys, where there is low resolution for the depth information. Additionally, as surveys are rarely done, depth information might be out-dated for some areas (Pe'eri et al., 2014). Moreover, the shallowest areas could contain uncertainties as survey vessels might struggle to reach these areas (Pe'eri et al., 2014).

For this study bathymetry was derived from multiple sets of Landsat satellite images and depths of around 5 m were reached every time. This makes the

results more trustworthy, whereas if different depth results were reached for each set, the results would be more questionable. Using the same algorithm with Landsat images, Pe'eri et al. (2014) reached depths of 6 m for their study, while the IHO-IOC Cookbook (International Hydrographic Organization and Intergovernmental Oceanographic Commission, 2018) derived depths of between 8-9 m in two separate examples. This indicates that the 5 m depth received from this study is reasonable.

There are, however, some studies using bathymetry derived from satellite images that obtained results that reached depths of 15-25 m (Stumpf et al., 2003; Purkis et al., 2010; Purkis et al., 2012; Purkis et al., 2015). In these studies there is emphasis put on the importance of more depth soundings to create better results from satellite derived bathymetry. Purkis et al. (2015) used four million depth soundings for a total area of ca. 6000 km^2, while Purkis et al. (2010) used more than 200 000 soundings in their study. For comparison, this thesis had around 40 000 depth points (excluding 0 m) with many depth values, especially in Aqaba, being very high (more than 50 m depth). These two studies, as well as Stumpf et al. (2003), used high-resolution satellite imagery from IKONOS or QuickBird. The resolution of these images is 4 m, whereas Landsat images only have a resolution of 30 m. This could help explain why the mentioned studies in this paragraph achieved higher depth results, while this thesis, along with Pe'eri et al. (2014) and the IHO-IOC Cookbook, derived depths of less then 10 m.

7 CONCLUSIONS

The analysis of the drainage in the southern Sinai Peninsula and its delivery of sediments to the coastal and shallow-water area, allowed to better understand the impact of the drainage on the development of the coral reefs growing on the fan deltas of the Gulf of Suez and Gulf of Aqaba. The main conclusions of this study are:

- Most of the area in the southern Sinai Peninsula is drained by only six large, lower-gradient catchments. These catchments deliver most of the sediments to the coastal areas during highly episodic flash flood events.
- The coastal fan deltas in the Gulf of Suez are larger in surface area than in the Gulf of Aqaba. Steep subaqueous slopes restrict fan progradation in the Gulf of Aqaba.
- Fringing coral reefs develop on coastal fan deltas along both Sinai coasts. Larger fan deltas have more coral reefs occupying the shallow-water area, explaining that the Gulf of Suez has more coral reefs colonising its shallow-water areas than in the Gulf of Aqaba.
- Most of the sediment derived from flash floods keep clear of the main bodies of coral reefs and are not deposited in the immediate shallow-water area, but rather a bit more distal in the area corresponding to 4-5 m depth. Sediments deposited in shallower areas and on the coral reefs are efficiently removed by marine currents and wave action.
- Rotated normal fault blocks in the Gulf of Suez and the absence of such blocks due to strike-slip in the Gulf of Aqaba is the primary control on the basin geometry, which control the size of coastal fan deltas, shallow-water area and areal size of coral reefs.
- The hyper-arid climate give warm, clear waters, ideal conditions for coral reef growth. The aperiodic flash flood event can be detrimental to coral reefs. The coral reefs grow on top of the coarse-grained sediments transported by the flash floods.

REFERENCES:

Allen, P. A., and Allen, J. R., 2013, Basin analysis : principles and application to petroleum play assessment, John Wiley & Sons, Incorporated.

Baker, J., Snee, L., and Menzies, M., 1996, A brief Oligocene period of flood volcanism in Yemen: implications for the duration and rate of continental flood volcanism at the Afro-Arabian triple junction: Earth and Planetary Science Letters, v. 138, p. 39-55.

Ben‐Avraham, Z., 1985, Structural framework of the gulf of Elat (Aqaba), northern Red Sea: Journal of Geophysical Research: Solid Earth, v. 90, p. 703-726.

Bosence, D., 2005, A genetic classification of carbonate platforms based on their basinal and tectonic settings in the Cenozoic: Sedimentary Geology, v. 175, p. 49-72.

Bosworth, W., 1995, A high-strain rift model for the southern Gulf of Suez (Egypt): Geological Society Special Publications, v. 80, p. 75-102.

Bosworth, W., 2015, Geological evolution of the Red Sea: historical background, review, and synthesis, The Red Sea, Springer, p. 45-78.

Bosworth, W., Crevello, P., Winn, R., and Steinmetz, J., 1998, Structure, sedimentation, and basin dynamics during rifting of the Gulf of Suez and north-western Red Sea, Sedimentation and Tectonics in Rift Basins Red Sea:-Gulf of Aden, Springer, p. 77-96.

Bosworth, W., Huchon, P., and McClay, K., 2005, The Red Sea and Gulf of Aden Basins: Journal of African Earth Sciences, v. 43, p. 334-378.

Cochran, J. R., 1983, A model for development of Red Sea: Aapg Bulletin, v. 67, p. 41-69.

Courtillot, V., Armijo, R., and Tapponnier, P., 1987, Kinematics of the Sinai triple junction and a two-phase model of Arabia-Africa rifting: Geological Society, London, Special Publications, v. 28, p. 559-573.

Cowie, P. A., Attal, M., Tucker, G. E., Whittaker, A. C., Naylor, M., Ganas, A., and Roberts, G. P., 2006, Investigating the surface process response to fault interaction and linkage using a numerical modelling approach: Basin Research, v. 18, p. 231-266.

Cowie, P. A., Gupta, S., and Dawers, N. H., 2000, Implications of fault array evolution for synrift depocentre development: insights from a numerical fault growth model: Basin Research, v. 12, p. 241-261.

Dawers, N. H., and Anders, M. H., 1995, Displacement-length scaling and fault linkage: Journal of Structural Geology, v. 17, p. 607,611-609,614.

Dewey, J. F., and Bird, J. M., 1970, Mountain belts and the new global tectonics: Journal of Geophysical Research, v. 75, p. 2625-2647.

Dullo, W.-C., and Montaggioni, L., 1998, Modern Red Sea coral reefs: a review of their morphologies and zonation, Sedimentation and Tectonics in Rift Basins Red Sea:-Gulf of Aden, Springer, p. 583-594.

Dupré, B., Dessert, C., Oliva, P., Goddéris, Y., Viers, J., François, L., Millot, R., and Gaillardet, J., 2003, Rivers, chemical weathering and Earth's climate: Comptes rendus - Géoscience, v. 335, p. 1141-1160.

Eliet, P., and Gawthorpe, R., 1995, Drainage development and sediment supply within rifts, examples from the Sperchios basin, central Greece: Journal of the Geological Society, v. 152, p. 883-893.

Eyal, M., Eyal, Y., Bartov, Y., and Steinitz, G., 1981, The tectonic development of the western margin of the Gulf of Elat (Aqaba) rift: Tectonophysics, v. 80, p. 39-66.
Fabricius, K. E., 2005, Effects of terrestrial runoff on the ecology of corals and coral reefs: review and synthesis: Marine pollution bulletin, v. 50, p. 125-146.
Farnsworth, K. L., and Milliman, J. D., 2003, Effects of climatic and anthropogenic change on small mountainous rivers: the Salinas River example: Global and Planetary Change, v. 39, p. 53-64.
Fick, S. E., and Hijmans, R. J., 2017, Worldclim 2: New 1-km resolution climate surfaces for global land areas: International Journal of Climatology.
FloodList, 2016, Egypt – Researchers Identify High-Risk Flooding Areas in Sinai Peninsula [Internet]: http://floodlist.com/africa/egypt-researchers-identify-high-risk-flooding-areas-sinai-peninsula, Accessed 30.05.2019.
Garfunkel, Z., 1981, Internal structure of the Dead Sea leaky transform (rift) in relation to plate kinematics: Tectonophysics, v. 80, p. 81-108.
Gawthorpe, R., and Colella, A., 1990, Tectonic controls on coarse-grained delta depositional systems in rift basins, Coarse-grained deltas, Volume 10, International Association of Sedimentologists, Special Publication 10, p. 113-127.
Gawthorpe, R. L., and Hurst, J. M., 1993, Transfer zones in extensional basins: their structural style and influence on drainage development and stratigraphy: Journal of the Geological Society, v. 150, p. 1137-1152.
Gawthorpe, R. L., and Leeder, M. R., 2000, Tectono-sedimentary evolution of active extensional basins: Basin Research, v. 12, p. 195-218.
Hay, W. W., Rosol, M., Sloan II, J., and Jory, D., 1988, Plate tectonic control of global patterns of detrital and carbonate sedimentation, Developments in Sedimentology, Volume 42, Elsevier, p. 1-34.
Hayward, A., 1982, Coral reefs in a clastic sedimentary environment: fossil (Miocene, SW Turkey) and modern (Recent, Red Sea) analogues: Coral Reefs, v. 1, p. 109-114.
Hermas, E., El-Magd, I. A., and Saleh, A., 2010, Monitoring the lateral channel movements on the alluvial fan of Wadi Feiran drainage basin, South Sinai, Egypt using multi-temporal satellite imagery: Journal of African Earth Sciences, v. 58, p. 89-96.
Hughes, G. W., Varol, O., and Beydoun, Z. R., 1991, Evidence for middle Oligocene rifting of the Gulf of Aden and for late Oligocene rifting of the southern Red Sea: Marine and Petroleum Geology, p. 354-358.
International Hydrographic Organization, and Intergovernmental Oceanographic Commission, 2018, The IHO-IOC GEBCO Cook Book: Monaco, IHO Publication B-11, p. 416.
Issar, A., and Gilad, D., 1982, Groundwater flow systems in the arid crystalline province of southern Sinai: Hydrological Sciences Journal, v. 27, p. 309-325.
Jackson, J., and Leeder, M., 1994, Drainage systems and the development of normal faults: an example from Pleasant Valley, Nevada: Journal of Structural Geology, v. 16, p. 1041-1059.
Jerlov, N. G., 1976, Marine optics, Amsterdam, The Netherlands, Elsevier.

Khalil, S., and McClay, K., 2002, Extensional fault-related folding, northwestern Red Sea, Egypt: Journal of Structural Geology, v. 24, p. 743-762.
Le Pichon, X., and Gaulier, J. M., 1988, The rotation of Arabia and the Levant fault system: Tectonophysics, v. 153, p. 271-294.
Leeder, M. R., and Jackson, J. A., 1993, The interaction between normal faulting and drainage in active extensional basins, with examples from the western United States and central Greece: Basin Research, v. 5, p. 79-102.
Leroy, S., Gente, P., Fournier, M., D' Acremont, E., Patriat, P., Beslier, M. O., Bellahsen, N., Maia, M., Blais, A., Perrot, J., Al‐Kathiri, A., Merkouriev, S., Fleury, J. M., Ruellan, P. Y., Lepvrier, C., and Huchon, P., 2004, From rifting to spreading in the eastern Gulf of Aden: a geophysical survey of a young oceanic basin from margin to margin: Terra Nova, v. 16, p. 185-192.
Manighetti, I., Tapponnier, P., Courtillot, V., Gruszow, S., and Gillot, P.-Y., 1997, Propagation of rifting along the Arabia‐Somalia Plate Boundary: The Gulfs of Aden and Tadjoura: Journal of Geophysical Research: Solid Earth, v. 102, p. 2681-2710.
Mckenzie, D. P., Davies, D., and Molnar, P., 1970, Plate Tectonics of the Red Sea and East Africa: Nature, v. 226, p. 243.
NASA, 2009, ASTER Global Digital Elevation Model V002 [Internet]: NASA LP DAAC; U.S. Geological Survey, https://lpdaac.usgs.gov/
NASA, 2019, Landsat 8 Overview [Internet]: https://landsat.gsfc.nasa.gov/landsat-8/landsat-8-overview/, Accessed 25.05.2019.
Nelson, R., Patton, T., and Morley, C., 1992, Rift-Segment Interaction and Its Relation to Hydrocarbon Exploration in Continental Rift Systems: AAPG bulletin, v. 76, p. 1153-1169.
Nir, Y., 1996, Sediment transport patterns of southern Sinai coasts and their role in the Holocene development of coral reefs and lagoons: Journal of coastal research, p. 70-78.
NOAA, and UKHO, 2019, iBoating Nautical charts [Internet]: http://fishing-app.gpsnauticalcharts.com/i-boating-fishing-web-app/fishing-marine-charts-navigation.html - 9.53/28.2381/34.4515 Accessed 25.01.2019.
Pe'eri, S., Parrish, C., Azuike, C., Alexander, L., and Armstrong, A., 2014, Satellite remote sensing as a reconnaissance tool for assessing nautical chart adequacy and completeness: Marine Geodesy, v. 37, p. 293-314.
Purkis, S. J., Harris, P. M., and Ellis, J., 2012, Patterns of Sedimentation In the Contemporary Red Sea As An Analog for Ancient Carbonates In Rift Settings: Journal of Sedimentary Research, v. 82, p. 859-870.
Purkis, S. J., Rowlands, G. P., and Kerr, J. M., 2015, Unravelling the influence of water depth and wave energy on the facies diversity of shelf carbonates: Sedimentology, v. 62, p. 541-565.
Purkis, S. J., Rowlands, G. P., Riegl, B. M., and Renaud, P. G., 2010, The paradox of tropical karst morphology in the coral reefs of the arid Middle East: Geology, v. 38, p. 227.
Purser, B. H., Soliman, M., Amp, Apos, and Rabet, A., 1987, Carbonate, evaporite, siliciclastic transitions in Quaternary rift sediments of the northwestern Red Sea: Sedimentary Geology, v. 53, p. 247-267.
Ravnås, R., and Steel, R., 1998, Architecture of marine rift-basin successions: AAPG bulletin, v. 82, p. 110-146.

Roberts, H. H., 1987, Modern carbonate-siliciclastic transitions: humid and arid tropical examples: Sedimentary Geology, v. 50, p. 25-65.
Roberts, H. H., and Murray, S. P., 1984, Developing carbonate platforms: southern Gulf of Suez, northern Red Sea: Marine geology, v. 59, p. 165-185.
Rowlands, G., and Purkis, S., 2015, Geomorphology of shallow water coral reef environments in the Red Sea, The Red Sea, Springer, p. 395-408.
Rowlands, G., Purkis, S., and Bruckner, A., 2014, Diversity in the geomorphology of shallow-water carbonate depositional systems in the Saudi Arabian Red Sea: Geomorphology, v. 222, p. 3-13.
Sahota, G., 1991, Geophysical study of the Gulf of Aden continental margins: geodynamic implications for the development of the Afro-Arabian Rift System, Ph.D. Thesis: University College of Swansea, United Kingdom.
Sharp, I. R., Gawthorpe, R. L., Underhill, J. R., and Gupta, S., 2000, Fault-propagation folding in extensional settings: Examples of structural style and synrift sedimentary response from the Suez rift, Sinai, Egypt: Geological Society of America Bulletin, v. 112, p. 1877-1899.
Steckler, M. S., and ten Brink, U. S., 1986, Lithospheric strength variations as a control on new plate boundaries; examples from the northern Red Sea region: Earth and Planetary Science Letters, v. 79, p. 120-132.
Stumpf, R. P., Holderied, K., and Sinclair, M., 2003, Determination of water depth with high‐resolution satellite imagery over variable bottom types: Limnology and Oceanography, v. 48, p. 547-556.
Syvitski, James P. M., and Milliman, John D., 2007, Geology, Geography, and Humans Battle for Dominance over the Delivery of Fluvial Sediment to the Coastal Ocean: The Journal of Geology, v. 115, p. 1-19.
Tarboton, D. G., Bras, R. L., and Rodriguez‐Iturbe, I., 1991, On the extraction of channel networks from digital elevation data: Hydrological processes, v. 5, p. 81-100.
Warrick, J. A., and Milliman, J. D., 2003, Hyperpycnal sediment discharge from semiarid southern California rivers: Implications for coastal sediment budgets: Geology, v. 31, p. 781-784.
Wilson, J. T., 1969, Static or mobile earth; the current scientific revolution: Tectonophysics, p. 600-601.
Young, M. J., Gawthorpe, R. L., and Sharp, I. R., 2000, Sedimentology and sequence stratigraphy of a transfer zone coarse‐grained delta, Miocene Suez Rift, Egypt: Sedimentology, v. 47, p. 1081-1104.